Ines Haynl, BSc

Analysis of soft materials using a new cryo atomic force microscope combined with an ultramicrotome

MASTER THESIS

For obtaining the academic degree
Diplom-Ingenieurin

Master Programme of
Technical Physics

Graz University of Technology

Supervisor:

Ao. Univ.-Prof. Dipl.-Ing. Dr.techn. Werner Grogger

Institute for Electron Microscopy and Fine Structure Research

Graz, November 2010

Abstract

Cryo atomic force microscopy (AFM) is a relatively new method that offers great possibilities to investigate soft materials, e.g. polymers, soft engineering materials, nanoliquids or biological materials for medical and pharmaceutical industry. In this master thesis results of AFM measurements done under cryo conditions are compared with those done at room temperature (RT) to point out new opportunities in material characterization.

To show the differences between RT-AFM and cryo-AFM on the one hand a Dimension^{TM} 3100 (Veeco Instruments, Santa Barbara, CA, USA) and on the other hand the specially designed AFM "Snotra" (Nano Scan Technology, Moscow, Russia) embedded in an ultramicrotome Leica EM FC6 (Leica Microsystems, Vienna, Austria) were used. The new cryo-application allows to do measurements immediately after sectioning the sample in the frozen state. Compared to known AFM devices it does not use a cantilever scanning the surface and a laser detection system, but it uses a quartz tuning fork to build a self-sensing and -actuating probe instead.

One crucial influence on the quality of sample surfaces and, as a consequence, measurements is sample preparation by ultramicrotomy. By comparing block faces after sectioning, done at room temperature and under cryo conditions in liquid nitrogen vapor atmosphere, it is easy to see how the quality of the surfaces and therefore the image is improved with the cryo technique.

Results are discussed by looking at experiments done with the two elastomeric block copolymers PA6/SAN and PA6/ABS to give a resume on the capacities of the device and the current state of the art in the ongoing development process. To complement, transmission electron microscopy (TEM) images are added because TEM is nowadays the most widely spread technique concerning the investigation of soft polymer blends. In addition a collection of other sample experiments is given to show the full potential of the new cryo-AFM device. This includes also three dimensional reconstructions done at room temperature as well as under cryo conditions.

Kurzfassung

Kryo-Rasterkraftmikroskopie (oder auch Atomkraftmikroskopie, AFM) ist eine relativ neue Methode, die es erlaubt weiche Materialien, wie z.B. Polymere, weiche Werkstoffe, Nanoliquids oder biologische Proben für die medizinische und pharmazeutische Industrie, zu untersuchen. In dieser Masterarbeit werden die Ergebnisse, durchgeführt am AFM einerseits im Kryo-Bereich und andererseits bei Raumtemperatur (RT), verglichen um die neuen Möglichkeiten in der Materialcharakterisierung hervorzuheben.
Um die Unterschiede zwischen RT-AFM und Kryo-AFM aufzuzeigen, wurden einerseits ein Dimension^{TM} 3100 (Veeco Instruments, Santa Barbara, CA, USA) und andererseits das eigens entwickelte Gerät "Snotra" (Nano Scan Technology, Moskau, Russland), eingebettet in ein Ultramikrotom Leica EM FC6 (Leica Microsystems, Wien, Österreich), verwendet. Die neue Kryo- Anwendung erlaubt Messungen sofort nach dem Schneiden der Probe im gefrorenen Zustand. Verglichen mit bekannten AFM-Geräten verwendet dieses keinen Cantilever, welcher die Oberfläche scannt, und kein Laser-Detektionssystem, sondern benutzt stattdessen eine Quarz-tuning fork, die als eigenständig betriebener und detektierender Sensor agiert.
Einen entscheidenden Einfluss auf die Qualität der Probenoberflächen und, als Konsequenz, der Messungen hat die Probenpräparation am Ultramikrotom. Vergleicht man das Probenstück nach dem Schnitt einmal bei Raumtemperatur und ein weiteres Mal unter Kryo-Bedingungen in der Atmosphäre von Dampf aus flüssigem Stickstoff, so kann man leicht sehen, wie die Qualität der Oberflächen und damit das Bild durch die Kryo-Technologie verbessert wird.
Ergebnisse werden anhand von gegenübergestellten Experimenten an den zwei elastomeren Block-Copolymeren PA6/SAN und PA6/ABS diskutiert um die Kapazitäten des Gerätes und den aktuellen Stand der Technik im laufenden Entwicklungsprozess aufzuzeigen. Ergänzend sind Bilder aus der Transmissionselektronen- Mikroskopie (TEM) beigefügt, weil TEM heutzutage die weitverbreitetste Technik bezüglich der Untersuchung von weichen Polymermischungen ist. Zusätzlich wird eine Sammlung aus Experimenten mit anderen Proben präsentiert um das gesamte Potential des neuen Kryo-AFM Gerätes aufzuzeigen. Dies beinhaltet auch dreidimensionale Rekonstruktionen gemessen bei Raumtemperatur und auch unter Kryo-Bedingungen.

Deutsche Fassung:
Beschluss der Curricula-Kommission für Bachelor-, Master- und Diplomstudien vom 10.11.2008
Genehmigung des Senates am 1.12.2008

EIDESSTATTLICHE ERKLÄRUNG

Ich erkläre an Eides statt, dass ich die vorliegende Arbeit selbstständig verfasst, andere als die angegebenen Quellen/Hilfsmittel nicht benutzt, und die den benutzten Quellen wörtlich und inhaltlich entnommene Stellen als solche kenntlich gemacht habe.

Graz, am ……. ……..
(Unterschrift)

Englische Fassung:

STATUTORY DECLARATION

I declare that I have authored this thesis independently, that I have not used other than the declared sources / resources, and that I have explicitly marked all material which has been quoted either literally or by content from the used sources.

……. ……..
date (signature)

Acknowledgment

This thesis was written at the Graz Centre for Electron Microscopy (ZFE), member of the Austrian Cooperative Research (ACR), within the scope of the project "3D-Mikroskopie von Polymeren und Biomaterialien" kindly supported by FFG, Austria (project no. 820223). At this point I would like to thank anybody who contributed to the success of this work.

Prof. Werner Grogger, my supervisor, I want to thank for the cordial acceptance at the institute and the work group, the confidence and freedom that was placed into my work, and the willingness to give backup in administrative as well as scientific problems.

My collaborator and the scientific responsible for this project at ZFE, Dr. Nadejda Matsko I would like to thank for the close collaboration, the enthusiastic support and the many discussions. Her help provided and her advices are also highly appreciated. Her interest and encouragement in the ongoing progress of the project have been a great aid.

Many thanks also to Prof. Hofer, the head of ZFE and FELMI (Institute for Electron Microscopy and Fine Structure Research, Graz University of Technology), for offering the possibility to work on this thesis at his institute.

The prototype of the cryo-AFM and the constant improvements and upgrades have been provided by Dr. Anton Efimov from Nano Scan Technology (Moscow, Russia) and his team. Special thanks to him for his significant contribution and his thoughtful comments and stimulating discussions.

I want to thank my colleagues at the institute, especially the chemical laboratories team for providing liquid nitrogen and machine maintenance, the mechanical team for supporting the upgrades of the cryo-AFM by providing self-constructions, and the media and administrative team for offering to work unhindered. Thanks also to Dr. Harald Plank for his fruitful discussions concerning conventional AFM techniques. And not to forget to thank all my colleagues for the friendly and amicable working atmosphere.

Special thanks go to my family, especially my mother, for the consecutive support during my whole studies and the work on this thesis, as well as Reinhold for his caring support and his readiness to help wherever it was possible.

Contents

List of Figures

1 Introduction

Nowadays investigation of soft materials of different types, such as polymers, soft engineering materials, nanoliquids etc., has to concentrate on the study of internal microstructures. These soft and sometimes hydrated materials can only be understood properly by knowing the bulk morphology which can be considered as the main factor that determines their properties. Looking at biological materials for medical and pharmaceutical industry the very same is necessary. So not only material scientists but also industry is strongly interested in a three dimensional investigation of soft materials concerning morphological, analytical and structural analysis.

At present transmission electron microscopy (TEM) is the most widely spread technique used for the investigation of such samples, e.g. polymer blends and composites. Further, most of our knowledge about cellular and polymer ultra- and microstructures is largely derived from TEM analysis.

In order to obtain this information using a TEM, first ultrathin sections have to be prepared. A routinely used preparation technique is ultramicrotomy operating at room temperature or under cryo conditions. Many soft polymers usually have a glass transition temperature T_g significantly below 0 °C and therefore these materials can be nicely sectioned by cryo-ultramicrotomy [1]. At adequate temperature ultramicrotomy permits the observation of the actual structure of a bulk material without causing changes of the microstructural properties of the samples [2].

After preparing ultrathin sections for TEM and placing them on a grid, they are ready for investigation with the microscope. TEM can be done at room temperature as well as under cryo conditions depending on what is best and required for each individual case. To prevent the section of a sample from undergoing structural changes caused by of heating between preparation and investigation, the whole procedure can also be done completely under cryo conditions.

TEM is well established and offers the best resolution available as well as information about crystallinity and chemical composition using electron diffraction, energy-dispersive X-ray spectroscopy (EDXS) analysis, electron energy-loss spectroscopy (EELS), energy filtered TEM (EFTEM) etc. This analytical interpretation can be done in a quantitative way to characterize the investigated section. In addition one can do tilt series of the section and a subsequent reconstruction in order to obtain a three dimensional view of the sample. Without tilting one gets the usual two dimensional projection which is provided by the microscope.
Image contrast is formed by electron scattering and most of the biomacromolecules as well as polymers mainly consist of light elements which scatter the electrons rather weakly. Consequently TEM images do not provide good image contrast. This can be improved by staining the sample but also does not allow to show all details of the structures of the samples because most of the protein macromolecule and polymer chains have low or selective stainability. In addition there exist indications that the staining process could change the native morphology of elastomers due to chemical reactions between side groups of polymer chains with the staining agent [3]. Image contrast can also be improved by applying higher voltages, but especially soft samples react very sensitively on beam damage [4], [2].
Conventinal AFM is also well established and offers possibilities of sample investigation operating in vacuum, ambient conditions or even aqueous or gaseous phase without needing special sample preparation like ultrathin sections or conductive surfaces of the samples. AFM is a surface characterization technique allowing in first case to investigate the topography of the sample surface quantitatively and does not suffer from projection or beam damage issues. In addition one can get at the same time information about mechanical properties through the detection of phase shifts. One can distinguish qualitatively between areas of different stiffness on the sample surface [5].
For AFM investigations the surface of the sample has to be really flat because the scanner is usually limited to a few microns of difference in height. Additionally the surface also has to be clean. Dust and other particles on the surface can influence the measurement to the point of interruption or even damage of the probe. Sample preparation for gaining such flat surfaces is done, like for TEM, with an ultramicrotome, but with the difference that for AFM not

the section but the remaining block face gets scanned which is much less deformable because the whole bulk stabilizes it.
AFM gives a three dimensional topography information of a single surface but no information about the internal three dimensional structure of the sample bulk. This was the motivation behind the idea of combining an AFM with an ultramicrotome which gives the possibility to obtain information about the location, architecture and mechanical properties of samples via tomography. By cutting a section off the block face, scanning afterwards the block face with AFM and again sectioning and scanning again, this procedure allows investigation of local changes within the sample and provides the whole microstructure in general when computing afterwards a three dimensional reconstruction of the area. Such a combination is already available on the market working under ambient condition at room temperature. It can be applied for serial section tomography of a wide range of biological and polymer materials, but only for hard samples that can be sectioned at room temperature without getting destroyed by compression and deformation [6].
Because of that a new AFM device combined with an ultramicrotome should be developed to operate not only at room temperature but also at cryo temperatures. Thereby the AFM is mounted directly in the cryogenic chamber of the ultramicrotome and stable measurements are possible for soft materials because any structural changes are avoided as the whole structure is stabilized by cold. Cooling is done by pumping liquid nitrogen into the chamber of the microtome and operation is done in the nitrogen vapor atmosphere. This device allows direct in-situ observation of the block face surface, three dimensional reconstruction, and collection of sections to make TEM investigations afterwards. One additional advantage is the possibility of operating in a wide range of temperatures (from -185 °C to 100 °C), because the cryogenic chamber may be also heated up. This can be used for studies of thermotropic structural changes and influence of temperature on mechanical properties accompanying melting, crystallization, or glass transition of polymers.
Of course this assembly has special requirements since a conventional AFM detection system using a laser and a photodiode to detect deflections of the cantilever is not suitable. The laser may lead to temperature changes on the sample surface and therefore ice contamination. This problem can be solved by replacing the cantilever with a quartz tuning fork with a sharp tip attached

to it building a self-sensing and -actuating probe.
The aim was to develop the described cryo-AFM combined with an ultramicrotome and to optimize its design and parameters to get satisfactory noise and resolution performance. This allows now the comprehensive analysis of soft and hydrated polymers such as elastomers and rubbers, thermoplastic and elastomeric composites, soft nanocomposites, nanoliquids, pharmaceutical substances, and biological objects with the new measurement methodology to resolve the ultrastructure of the samples without any change of structure due to temperature changes between sectioning and measuring. Besides scanning a single block face surface, tomography can be done as well. In order to complement this technique, TEM can help to interpret the results for instance by elemental information.
During the work for this thesis it was a continuous developing and optimizing process on the device and the thesis itself tries to point out the advantages of the cryo-AFM technique with a view to investigation of soft materials and analysis of the results. Quality improvement of sectioning is also shown by comparison of section and block face preparation at room temperature and under cryo conditions respectively. The results are supplemented by TEM images.

2 Methods and Materials

This chapter gives a short overview of methods and materials used during the progression of this thesis. It starts with atomic force microscopy and afterwards includes ultramicrotomy, ending up with a short introduction to each of the two main samples used for analysis later on.

2.1 Room Temperature Atomic Force Microscopy

2.1.1 Principles and Modes

Atomic force microscopy (AFM) is only one type of scanning probe microscopy (SPM) and can be separated in a broad area of different modes and techniques. It is based on the interaction of forces between a tiny tip and the surface of a specimen. Invented by Binnig et. al. in 1986 [7], we nowadays distinguish between contact, intermittent-contact (tapping) and non-contact mode (see section 2.1.1.1 to 2.1.1.3). Until the tip gets in contact with the sample, the force is attractive and in contact mode repulsive forces are measured between the tip and the sample. One gets images that are related to the surface topography, because the tip-to-sample force is proportional to the local electron density of the top surface atoms [8].
Using an AFM, the sample surface gets scanned by a probe consisting of a cantilever with a sharp tip on its end. Spring constant values of the cantilevers usually lie between 0.01 N m^{-1} and 50 N m^{-1} for commercially microfabricated Si and Si_3N_4 probes, where soft ones are used for contact mode and more rigid ones are preferred for tapping mode because of the need to withdraw the tip from the sample after each tap. Due to the forces between sample and tip

mentioned before, which could be either attractive or repulsive, the cantilever starts to bend in contact mode or its oscillation amplitude gets damped in the tapping mode. This is monitored by an optical system. A laser is measuring the deflection and torsion of the cantilever by reflecting its light from the beam focused on the back side of the tip to a four-quadrant photodetector. One can either move the sample or the cantilever, controlled by a piezoelectric drive in the horizontal plane and by a feedback mechanism for the vertical motion, to scan the surface [5]. Figure 2.1 shows the described assembly thereby using a scanner to move the sample.

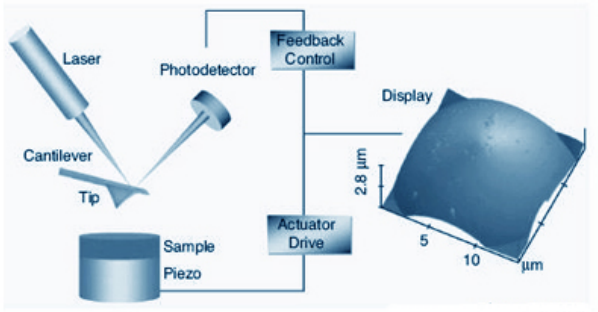

Figure 2.1: Assembly of an AFM where the sample is moved and the cantilever is fixed. [Fig. from [9]]

We should not forget to mention two of the most important facts why AFM became so important: First it is able to operate in different environments like e.g. vacuum or ambient conditions and second there is no need for conductive surfaces, which makes the method attractive for applications where these conditions are necessary. Atomic resolution may only be reached under vacuum conditions but you still get excellent images up to atomic resolution in air or even in liquid or gaseous phases. Combining these facts it gets obvious that AFM can play an important role in investigating insulators such as polymers and biological samples.
During the work on the thesis only tapping mode was used for doing both, RT-AFM and cryo-AFM, but to complete the introduction, a few words about the three possible modes should be given:

2.1.1.1 Contact Mode

In contact mode the tip is in permanent contact with the sample scanning the decided region. One should be sure not to deform the surface by using too large forces in order to get the right information about the topography of the sample. So, for the right interpretation of measurements and images, it is always better to apply different forces and to compare the results. This is called the constant-force mode. For soft materials it is necessary to use a higher lateral force because of the larger penetration of the tip into the sample but for very high forces one should also be very careful. It may happen that the image contrast will not contain that much information about topography but more information about variations of surface stiffness. Usually this is because the observed deflection amplitude is larger when the tip interacts with hard surface regions than with softer ones. This also requires attention and experience concerning the right interpretation of the results. Usually the tip-to-sample force in contact mode at ambient conditions is between 10 nN and 100 nN and can only be classified as low or high by comparison with the stiffness of a sample under investigation [5].

2.1.1.2 Non-Contact Mode

Non-contact mode uses either amplitude or frequency modulation. So, while scanning the surface without touching it with the tip, the system recognizes changes in the topography as changes of the behavior of the cantilever due to its interaction with the sample. Therefore the cantilever is oscillating at or close to its resonance frequency and the oscillation amplitude, the phase and the frequency itself are modified by interaction forces between the tip and the sample so that force gradients can be detected.
Because we are able to measure frequency with very high sensitivity, we can use stiff cantilevers that offer stability also very close to the surface. As a result, this technique was the first at AFM that provided true atomic resolution in ultra-high vacuum (UHV) conditions [10].
In amplitude modulation the change of the phase of oscillation is the most important and it is used to discriminate between different types of materials

on the surface. It can be used also in the tapping mode and it will be discussed later because it will get very important for measurements done for this thesis.

2.1.1.3 Tapping Mode

The big advantage of tapping mode, in particular while operating with soft samples, is that one applies much less force because of short, intermittent contacts that minimize the inelastic deformation of the sample. Force can be varied by changing the driving amplitude A_0 and/or the set-point amplitude A_{sp}, which are the two most important parameters in this case. The driving amplitude is the amplitude of the free oscillating cantilever, while set-point amplitude refers to the damped amplitude during tapping the sample surface. Logically, by increasing A_0 and/or decreasing A_{sp}, the effective tip-to-sample force also increases [11].
In case of tapping mode the frequency and phase of the oscillating cantilever are very sensitive to the tip-to-sample interaction force. One can describe the vibrating probe as a harmonic oscillator. This description leads to the result that repulsive tip-to-sample force interactions cause a shift of the resonance frequency to higher frequencies and attractive forces, on the opposite, decrease resonance frequency [12]. Therefore the images of shifts in phase and frequency offer additional information about the sample surface and its properties. More details concerning phase contrast can be found in section 2.1.4.
As mentioned before in the section about the non-contact mode, the phase images are very useful. They are often recorded simultaneously with the height images and also the amplitude images and provide the best contrast of fine morphological and nanostructural features due to their high sensitivity to surface imperfections. Even local variations of mechanical properties on surfaces can be detected by looking at the phase image. To distinguish between so called hard, moderate, and light tapping one calculates the set point ratio r_{sp} as follows:

$$r_{\mathrm{sp}} = \frac{A_{\mathrm{sp}}}{A_0} \tag{2.1}$$

Using high A_{sp}/A_0 ratios (0.8 to 0.9) will not show much difference in phase on different components with different grades of stiffness, because the phase shifts have similar magnitude. This adjustment is called "light tapping" due to small tip-to-sample force interactions. With decrease of A_{sp}/A_0, the phase curves behave differently. At A_{sp}/A_0 in the 0.3 to 0.8 range, known as "moderate tapping", one can observe greater differences between different components concerning the phase shifts. This can be explained either by adhesion between the tip and the sample caused by increasing of the tip-to-sample contact area or by viscoelastic effects. Scanning harder materials leads to large positive frequency and phase shifts, both measured with respect to the frequency and phase of the freely oscillating cantilever, in comparison with scanning soft materials. This is why phase images are important in investigating samples with different areas of stiffness. Imaging performed at set point ratios below 0.3 is known as "hard tapping" [5].

2.1.2 The Feedback System

Concerning the feedback mechanism there is a good description found in [8] which says that the four-segment photodetector is used by the electronic feedback system to do surface imaging. The four segments are linked to each other to get pairs of vertical segments and horizontal ones. The former are used for measurement of the cantilever deflections caused by normal tip-sample force, the latter are used for measurement of the cantilever torsion that exists due to lateral tip-sample forces. The resulting signal, known also as the error signal, is the difference between the current value of the normal tip-sample force and its set-point value which is chosen to adjust the vertical probe-sample separation and to keep the tip-sample force interaction constant during scanning.
To optimize the choice of the error signal, in order to get a stable image with maximum noise reduction and minimum instability fluctuations during scanning, a proportional-integral-derivative (PID) controller is used. The proportional term as well as the integral and the derivative term can be adjusted by the operator. The three correcting terms sum up to a variable $V(e)$ as a

function of the error e, which afterwards changes the error signal by its value. The function can be written in the parallel form (equation 2.2) or the ideal form (equation 2.3).

$$V(e) = K_\mathrm{P} + K_\mathrm{I}\frac{1}{e} + K_\mathrm{D}e \tag{2.2}$$

$$V(e) = K_\mathrm{P}\Big(1 + \frac{1}{T_\mathrm{I}e} + T_\mathrm{D}e\Big) \tag{2.3}$$

$$\text{with } K_\mathrm{I} = K_\mathrm{P}\frac{1}{T_\mathrm{I}}$$

$$\text{and } K_\mathrm{D} = K_\mathrm{P}T_\mathrm{D}$$

were K_P is the propartional gain, K_I is the integral gain and K_D is the derivative gain. T_I is the integral time constant and T_D is the derivative time constant. The proportional term provides a change to the output that is proportional to the current error signal. The integral term is proportional to both, the magnitude of the error and the duration of the error, and reduces steady-state errors because it eliminates the proportional offset over time by looking at the accumulated offset. The derivative term calculates the rate of change by determining the slope of the error over time [13].
Regarding the feedback system the two AFM devices used to behave differently: For the conventional AFM operated at room temperature (Dimension™ 3100) only settings for the intergral and the proportional term are possible, this means a PI controller is provided. It follows the rule of thumb that the proportional value has to be twice as high as the integral one. The cryo-AFM ("Snotra") is equiped, on the other hand, with a PID controller which requires different rules. During the landing procedure of the tip on the sample all three values have to be set to their maximum to ensure that the system recognizes the surface of the sample. After landing and establishing a contact between the probe and the specimen, the integral gain is the parameter that is most sensitive to instability during scanning and has to be set to relatively small values. The correct adjustment of the feedback parameters can be estimated by looking at the resulting images and reducing of fluctuating oscillations to a minimum that do not belong to information of the scanned surface.

2.1.3 Acting Forces

As one can see in figure 2.2, we get different forces between the tip and the sample at different distances and therefore also different signals. Attractive forces change into repulsive forces when the tip gets in contact with the sample surface. This curve is called the Lennard-Jones potential and follows equation 2.4, with interaction constants A and B and the interaction energy w as a function of distance r. The attractive contribution derives from van der Waals forces at long ranges, the repulsive contribution is called the Pauli repulsion, also known as exchange interaction, and acts in the short range due to overlapping electron orbitals.

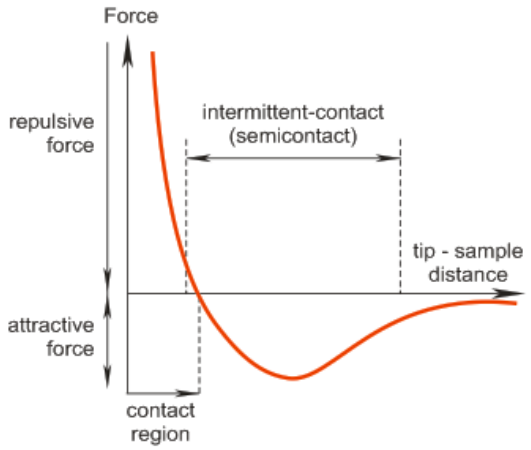

Figure 2.2: The force acting between sample and tip depends on the distance between them. [Fig. from [14]]

$$w(r) = -\frac{A}{r^6} + \frac{B}{r^{12}} \tag{2.4}$$

Van der Waals forces are the most contributing part to acting forces between the probe and the sample, but one part also derives from adhesion between those two different materials. To measure adhesion of the sample, so called force curves are recorded. They describe the probe deflection in contact mode or the variations of the cantilever amplitude in tapping mode and are plotted versus the vertical travel of the tip (see figure 2.3). One can recognize from the caption of figure (a) how the tip gets influenced by the sample. The reason for

the fact that the tip is stuck to the sample is capillary force and the needed pull-out force causes the hysteresis in the curves that can be used to measure adhesion [8]. The contact angle when advancing is often found to be larger than the receding one and the resulting hysteresis, as already mentioned, appears due to the irreversibility of this process. This includes energy dissipation but also the effect of capillary condensation on adhesion. Capillary condensation of water around surface contact sites can have a strong influence on adhesion forces since they are very sensitive to the presence of humidity in the surrounding atmosphere [15].

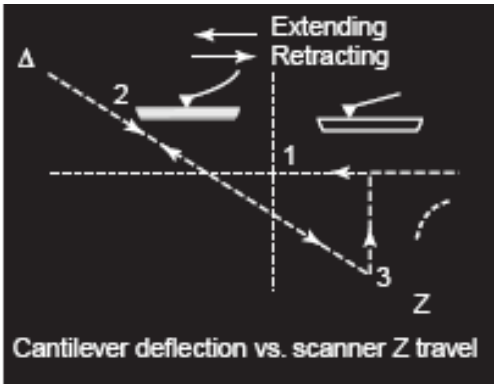

(a) When the sample approaches the tip (←, right to left) attractive force (point 1) slightly bends the probe down (△, cantilever deflection). Further sample travel will induce upward bending of the cantilever caused by repulsive forces (point 2). On reverse travel (→), the tip is stuck to the sample until the probe spring stiffness overcomes the adhesion/capillary forces (point 3).

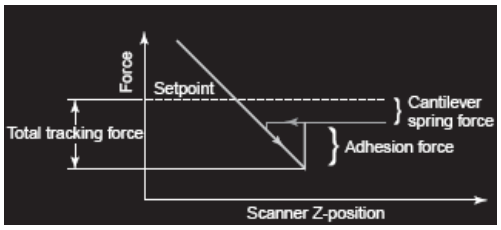

(b) Scheme of different forces acting on a probe: The total tracking force is the force between the set point and the sample surface, whereas the adhesion force can be measured as the force needed to retract the tip from the sample and is the difference between the total tracking force and the cantilever spring force.

Figure 2.3: Force curve and description of the behavior of the probe in respect of the sample distance (a) including the schematic characterization of the different forces (b). [Fig. from [8]]

2.1.4 Phase Contrast in Tapping Mode

As already mentioned in section 2.1.1.3, the phase contrast image in tapping mode strongly depends on the force one applies to the sample by choosing the amplitude parameters A_0 and A_{sp}. There has been a long scientific discussion about the phase contrast and it is generally accepted that the brighter regions usually correspond to harder materials because the interaction of tip and sample is dominated by repulsive forces. But there also exist opposite observations, so that the phase data evaluation is not always straightforward. Studies [16] showed some new explanations concerning the contrast-reversal in AFM phase images:
When the tip approaches the sample using tapping mode, the amplitude and the phase of the cantilever change. Due to the feedback system the amplitude is maintained at a constant level. If now the tip reaches a surface region where the amplitude gets more damped, the feedback control moves the sample and the tip further apart from each other and thus this area is recorded as higher topography. At the same time the system records the phase shift $\Delta\varphi$ with respect to the freely oscillating cantilever and produces a phase image.
One model that tries to explain the phase data uses an energy model that gives a relation between the phase angle φ, the amplitude A and the average power dissipation $\bar{P}$:

$$\bar{P} = \frac{kA^2\omega}{2Q}\left(\frac{A_0}{A}\sin\varphi - 1\right) \tag{2.5}$$

where k is a constant, Q is the quality factor, A_0 is the amplitude of the free oscillating cantilever, and ω is the natural resonance frequency. Due to the sine-dependency of the phase there are two explanations for the phase contrast:

- Using a constant amplitude for scanning, the $\sin\varphi$ is directly proportional to changes of the energy dissipation. The consequence for a two-phase system is that the region with the phase angle closer to the free phase, which is 90°, has the higher energy dissipation.
- The sine function is symmetric around 90° and symmetric jumps from phase $> 90°$ to $< 90°$ are not caused by energy dissipation but by switch-

ing between attractive and repulsive forces between the tip and the sample.

The total force between the tip and the sample F_t is the sum of attractive forces F_a and repulsive forces F_r:

$$F_t = F_a + F_r \tag{2.6}$$

If the tip touches the surface of the sample, even when the sample is flat, the indention of the soft phase is deeper. Under light tapping conditions the total force is dominated by attractive forces, the deep indention leads to even higher attractive forces, and combining this with a longer contact time results in a larger amplitude damping and therefore a brighter domain in the height image. This is exactly the opposite of what is expected, because now soft regions, that have been indented deeper, seem to be higher. This leads to the result that AFM height images are not necessarily reflecting the surface topography but sometimes show the lateral differences in tip-indentation depth. Because of this fact it is also obvious that even almost completely flat surfaces may also show topography.
Under these light tapping conditions the phase differences between hard and soft domains are quite similar and above 90° and the region with the larger energy dissipation, which is the soft one, has a less negative phase shift and looks brighter in the phase image.
Increasing the tapping force induces increasing of the repulsive force whereas the repulsive force increases much faster on the hard domains besause they are less deformable. Furthermore the attractive force in the soft regions counterparts the repulsive one because with increasing deformation the tip gets more contact area. In this case it happens that the total force F_t in the hard region becomes repulsive and in the soft region it is still attractive and one gets an inversion of the phase image.
Finally reaching moderate tapping conditions, repulsive forces should dominate in both domains and in this case the harder material shows larger decrease in amplitude and appears brighter in the image [16]. All these explanations are valid under the assumption that one works under ambient conditions and under consideration that cantilever forces can be in a wide range and materials

can behave in different ways.
Because of the fact that the phase contrast can get reversed, hard surface regions are brighter instead of darker choosing specific parameter values for A_0 and A_{sp}. This happens in conditions from moderate to hard tapping, which are prefered to use because they give a better contrast of components with different stiffness.
In theory this seems to be easy, but in reality there exists the problem to find parameters at which the phase contrast is stable. Only choosing a set point value where the phase is the same for forward and backward scanning leads to true information in the phase image. Selecting A_{sp} that is related to two phase values close to each other causes a stable phase image too but differs in the two phase images of trace and retrace. And choosing A_{sp} linked to two completely diverged phase values yields an unstable phase one cannot work with properly.
There are various reasons which are still not understood very well why the phase in forward and backward motion during scanning only fits badly. It is known that there exist dependencies on amplifiers of the signal in the controller, the used algorithms to reproduce the signal, the angle of the tip that touches the surface of the sample, the stiffness of the tip (For example using hard tips leads to a phase that is much more stable than using soft tips while scanning soft samples.), and so forth.
The best way to be sure to get the right phase data is offered in three suggestions:

- Put known hard particles (e.g. gold) on one side of the sample and choose parameters in a way that the hard particles are definitely bright in the phase image and the soft sample appears dark. Then change to a different place where the surface is clean and scan with the same parameters.
- Take a look at rheology studies of the materials you like to investigate and find out which one is harder. Choose parameters that show the hard domains brighter than the soft ones.
- If you cannot see any more topography information in the phase image, and if the phase curves, and also the phase images, look the same for trace and retrace recording, parameters are also chosen properly.

The right interpretation of images, done with AFM, needs experience and understanding of the system and the sample. Like other microscopic methods, AFM is not free of artifacts that could be caused by many factors, e.g. the choice of nonoptimal imaging parameters such as set-point, scan velocity or feedback gains. A bad tip caused either by manufacturing defects, material of the sample that got stuck on the tip, or even tip damage can be the reasons for artifacts too [8].
Starting to measure samples in a conventional RT-AFM induced some nice examples of what should be paid attention at. This means on the one hand operating with the system itself and on the other hand choosing the right parameters for each sample.
The AFM used was a Dimension^{TM} 3100 from Digital Instruments Veeco (Santa Barbara, CA, USA) enclosed in a glove box under gaseous nitrogen atmosphere at room temperature. This helps to reduce the water contamination on the surface of the sample. The cantilevers used were NSG 10 Golden Silicon Probes from NT-MDT (Moscow, Russia).

2.1.4.1 Example 1: Phase Contrast Reversal on PA6/ABS

Figure 2.4 shows results produced with different settings for A_0 and A_{sp} and therefore different set point ratios r_{sp}. Figure 2.4 (a) results from chosen parameters A_{sp}=1 000 mV and A_0=450 mV whereas for measuring figure 2.4 (b) parameters A_{sp}=4 000 mV and A_0=2 800 mV have been set. Since harder components should appear brighter than softer ones and ABS is softer than the polyamide 6 matrix (for explanation read section 2.5), figure 2.4 (a) shows the proper color coding. Even if the parameters are chosen to get a stable phase, the images should be regarded with suspicion.
The images have been recorded one after another on the same day without new sample preparation in between. This means that sectioning temperature was -120 °C in both cases and does not influence the resulting phase contrast. The phase contrast only depends on chosen landing and scanning parameters. Additional description and interpretation of what can be learned from such AFM images can be found in chapters 3 and 4 in more detail.

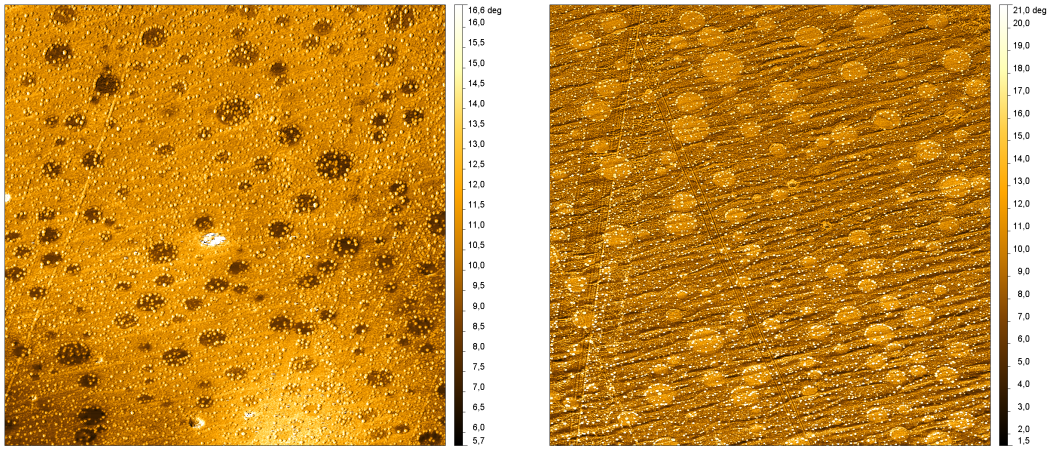

(a) Softer regions appear darker. This is how it should look like. (15.63 µm x 15.63 µm scan; r_{sp}=2.22)

(b) Softer regions appear brighter under changed conditions due to contrast-reversal. (15.63 µm x 15.63 µm scan; r_{sp}=1.43)

Figure 2.4: Comparison of two phase images taken from a PA6/ABS sample. One time the softer regions (the round ABS particles embedded in the polyamide matrix) appear darker and one time brighter due to different parameters of the amplitudes during measuring.

2.1.4.2 Example 2: Missing Phase Contrast on PA6/SAN

Comparing two different phase images of another sample, PA6/SAN, allows us to see some more important aspects. In figure 2.5 the first thing to recognize is again phase contrast which is visible only in image (a) but not in (b). The round dark regions in (a) are SAN while the matrix is again polyamide 6 [17]. So both samples, PA6/ABS and PA6/SAN, consist of round, spherical particles of either ABS or SAN embedded in the PA6 matrix. SAN domains are also much softer than the polyamide 6 matrix and so phase contrast with darker SAN particles and brighter matrix is correctly shown in figure 2.5 (a). On the other hand figure 2.5 (b) does not show any phase contrast although both times the sample surface was sectioned under the same conditions under -120 °C and measured with exactly the same set point ratio r_{sp} = 0.5 but different values of A_{sp} and A_0. For (a) A_{sp}=2 500 mV and A_0=5 000 mV and for (b) A_{sp}=2 000 mV and A_0=4 000 mV have been chosen. So once again phase contrast does not always appear in the same way and for a correct interpretation a lot of experience and patience is needed from the operators side.

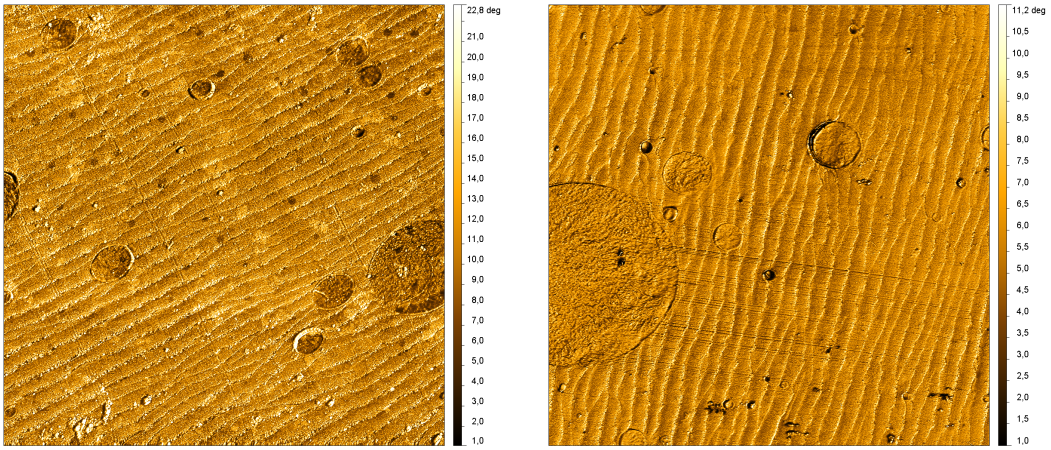

(a) Phase contrast is visible. (14.58 µm x 14.58 µm scan; r_{sp}=0.5)

(b) No phase contrast is visible. (14.58 µm x 14.58 µm scan; r_{sp}=0.5)

Figure 2.5: Comparison of two phase images taken from a PA6/SAN sample. In (b) the phase contrast is not apparent at all while in (a) parameters are chosen perfectly. Both images were taken after cryo-sectioning at -120 °C.

2.2 Cryo Atomic Force Microscopy

2.2.1 Motivation

The reason to use an AFM under cryo conditions is the need to investigate biological and polymer materials which are both soft and quite similar in their composition and behavior. Both include chains and parts that appear in periodic sequences. As already mentioned in chapter 1, these soft samples usually have a glass transition temperature significantly below 0 °C. In order not to change the ultra- and microstructure either by sample preparation or by measuring, cryo temperatures are recommended. Operating the AFM in a liquid nitrogen vapor atmosphere offers the needed temperature ranges that are necessary to investigate soft materials. As a consequence one has to cope with vapor turbulences and the need of a new detection system which is explained in the following section.

2.2.2 Principles and Differences Compared to RT-AFM

The main difference between the AFM used at room temperature and the one used at low temperatures in liquid nitrogen vapor atmosphere is the detection system itself. Whereas RT-AFMs usually use a cantilever scanning the sample surface and a laser combined with a photodiode, in a cryo-AFM a laser can influence the sample surface under cryo conditions. Installing an optical microscope inside the microtome chamber for adjustments would also lead to space problems and further optics would be crucially disturbed by vapor turbulences. In our case we use a quartz tuning fork instead to build a self-sensing and -actuating probe. Glueing a sharp tungsten tip on one of the prongs of the fork, the fork will oscillate when applying a voltage to the quartz crystal and no further external device is necessary. The tungsten tips get etched electrochemically and can be sharpened afterwards with a focused ion beam (FIB). The detection of the oscillations and especially their shift in frequency is done electrically. This is called "Qplus sensor" when fixing thereby the "empty" prong [18]. Figure 2.6 shows a scanning electron microscopy image (SEM) of a self made quartz tuning fork.

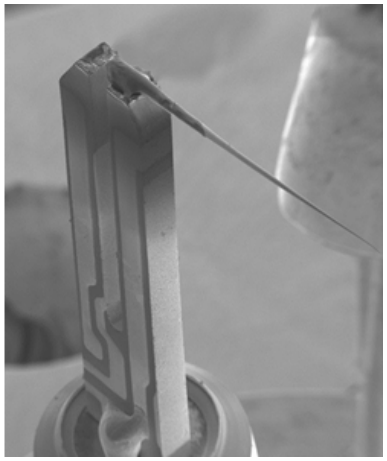

Figure 2.6: SEM image of a quartz tuning fork with a sharp tungsten tip glued on it. [Fig. from [19]]

2.2.2.1 The Tuning Fork and Its Q-Factor

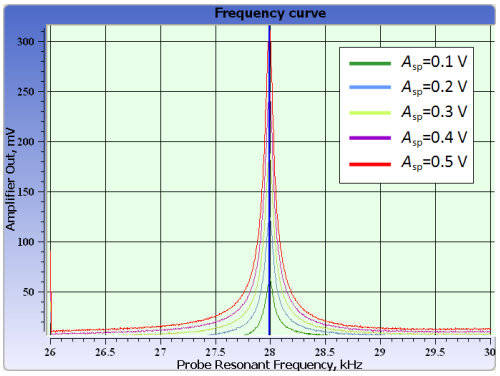

(a) Resonance curves measured without amplification

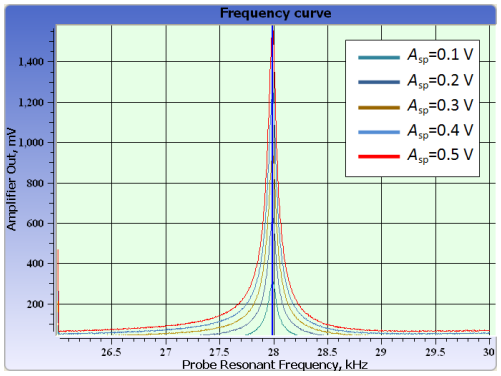

(b) Resonance curves measured with five-fold amplification

Figure 2.7: Resonance curves of a tuning fork with a 50 µm tungsten wire glued on it. Measurements were done at room temperature in air.

Using such a quartz tuning fork, the quality factor (or Q-factor) is the most important parameter to be considered because it influences the resolution of the measured image as well as the feasible scanning velocity. It is defined as the ratio of energy stored in the resonator to the energy lost during each oscillation period and in this way describes how the damping of the resonator behaves. Due to the stiffness of quartz one can reach high Q-factors of tens of thousands at the fundamental frequency of 32 768 Hz under vacuum conditions. If one uses the tuning fork in air, the energy losses get higher because of friction and the Q-factor drops to a few thousand [20].

It still has to be proven how the length, thickness, stiffness and mass of the tungsten tip as well as its position on the prong influence the Q-factor. This is necessary to improve the Q-factor especially in cryo conditions to ensure good resolutions of images.

The disadvantage of high Q-factors is the very slow response of the oscillation amplitude or phase [21]. Hence, cantilevers with high Q-factors are more sensitive to small force variations, whereas those with low Q-factors can be used for precise height measurements in tapping mode and they are also more suitable for fast scanning [8].

To improve the signal of the resonance curve it can be amplified with the help of an amplifier. Image 2.7 shows the comparison of signals measured at

different driving amplitude levels, once with and once without amplification. Thereby the Q-factor stays more or less the same at a value of Q=223, so the driving amplitude value as well as the amplification do not influence it.

2.3 (Cryo-)Ultramicrotomy

2.3.1 Principles and Sample Preparation

Before scanning sample block faces using AFM, sample preparation is necessary to ensure flat surfaces. This can be done by ultramicrotomy. Sample preparation itself is important because it has a crucial influence on the final quality of the sections and of the block face at the same time. It is essential to get as flat and homogenous sample surfaces as possible, because the surface roughness of the sample can be a practical limitation for AFM. The reason is the limited vertical range of the piezo tube, which is, in most tubes, only a few micrometers. Furthermore it could get difficult to scan fine features with steep slopes because of imperfections of the feedback and the crosstalk between vertical and lateral motions of the actuators [22].
Ultramicrotomy can be used at room temperature, but as we want to investigate soft materials cryo conditions are necessary. Since the glass transition temperature of soft materials is low, the structure of these samples would get destroyed by cutting them at a temperature higher than T_g (see chapter 1). Materials can be nicely sectioned only at temperatures 10 to 20 degrees lower than T_g [22].
The technical principles behind an ultramicrotome are shown in figure 2.8. The sample, fixed on its holder, gets cut by moving it with the ultramicrotome arm first towards the knife and then from the top down to cut a slice with the thickness set up before. Afterwards the arm retracts and starts again with approaching for the next cut. Figure 2.8 already contains the AFM scanner with the probe to scan the sample surface after each section. We will discuss this combination in more detail later on.
It is not just necessary to choose an adequate temperature for each sample,

further it is important to make the cutted surface as small as possible (preferably 1 mm^2). This is done by using a razor blade and trimming the sample into the shape of a pyramid starting to cut the tip afterwards with a diamond knife. The sample also has to be mechanically fixed on the holder to prevent thermal drift. If the knife edge has some imperfections, knife marks may appear on the sample surface in the cutting direction. Cracks are found predominantly perpendicular to the cutting direction and the sample itself as well as the section cut from it are deformed parallel to the knife edge [23]. As Steinbrecht et. al. write in [23], the process of sectioning a sample at cryo temperatures is not fully understood yet:

> *"There is an extended discussion on the nature of the cryosectioning process, particularly on the question whether sections are generated by local melting or by cleaving without any significant increase of temperature. The answer to this question is not only of academical interest, but would imply important consequences for the concept of cryoultramicrotomy. If sections would transiently melt during cutting, then the risk of redistribution of diffusable substances would increase and recrystallization of ice could affect the ultrastructure. Furthermore, an understanding of the cryosectioning process is expected to help in avoiding or at least reducing the observed deformations."*

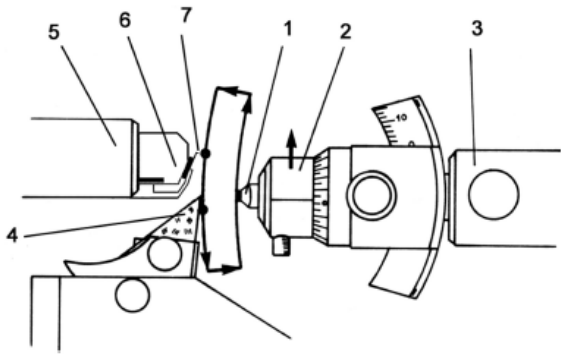

Figure 2.8: Principle scheme of the AFM tomography setup: 1 - sample, 2 - sample holder, 3 - movable ultramicrotome arm, 4 - ultramicrotome knife, 5 - AFM scanner, 6 - probe holder, 7 - AFM probe. [Fig. from [6]]

2.3.1.1 Sample Preparation for TEM Investigation

To investigate samples using TEM the samples themselves have to be as thin as possible to ensure that the electrons can travel through. TEM preparation is linked to AFM preparation and is done with the ultramicrotome as well. While the sectioned and therefore flat surface of the block face gets used for AFM analysis, the thin section can be collected for TEM studies. To catch a section, cut before under cryo conditions, a wire loop wetted with a solution of 50% Dimethyl Sulfoxide (DMSO) and 50% distilled water has to touch it and immediately attracts it. The loop holding the section has to be put into a dish filled with distilled water to select afterwards the best sections under an optical microscope and to put them again with the help of the loop on a TEM copper grid coated with a carbon film. Sections are either grey or they show interference colors depending on their thickness. Afterwards investigation of the sample can be started. To ensure better contrast, especially studying copolymers, staining can be applied. Osmium Tetroxide (OsO_4) together with the sections on the grids in a wet bath for some hours is a soft staining method. Of course a lot of other different sample preparation methods exist, but since these methods are not used during experimental work for this thesis they will not be explained in more detail. For further information [24] gives an overview concerning this topic.

2.3.2 Combination with AFM

Combining both systems, AFM and ultramicrotome, this is a technique that allows to make in-situ AFM measurements without temperature change between sectioning and scanning and to record the 3D structure in one go. Besides doing this section-picture-section procedure and combining the images to a three dimensional reconstruction of the sample, one can also collect the sections and investigate them with a transmission electron microscope (TEM). These complementary sets of AFM and TEM images allow to get informations from both techniques and to combine them for better understanding. Another advantage of the new AFM system is the possibility to detect areas of interest in samples with good efficiency by scanning the surface after each section.

Figure 2.8 illustrates the combinated measuring and sectioning system: After doing a section and approaching with the ultramicrotome arm towards the knife to section the sample once again, the arm stops at a defined position in front of the AFM scanner so that the sample surface can be investigated [6]. The described device is called NTEGRA Tomo from NT-MDT (Moscow, Russia) and found already application in science ([25], [26]). Requirements for the cryo-AFM system have already been mentioned above in section 2.2 and motivation therefore is explained in detail in the introduction (chapter 1).

2.4 Characteristics of Polyamide6/SAN

PA6/SAN is a polymer blend of polyamide 6 and styrene-acrylonitrile, which means to be a mixture of these two different species of polymers, combining also their properties. Because polymers are high molecular mass materials, they have a low entropy of mixing and therefore mixing is unfavorable. So most compositions of polymers are immiscible which leads to a multi-phase morphology [17]. As SAN is a copolymer, formed from more than one type of repeat unit, this multi-phase morphology is known as a block copolymer. Such blends lead to new properties compared to properties of a single SAN copolymer or a PA6 polymer [27]. The molecular formula for SAN is $(C_8H_8)_n(C_3H_3N)_m$ and its chain structure is shown in figure 2.9, the molecular formula of PA6 is $(C_6H_{11}NO)_n$ and this chain structure is displayed in figure 2.10.

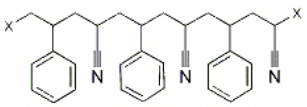

Figure 2.9: Image of a SAN chain with repeating styrene C_8H_8 and acrylonitrile C_3H_3N parts. [Fig. from [28]]

Because SAN is impact resistant, has a good hardness and scratch resistance, this material is used for cases of domestic appliances but also for toys. The use of PA6/SAN blends for industrial application is unknown, except for materials research (e.g. [29], [17]) or examination of measurement methods.

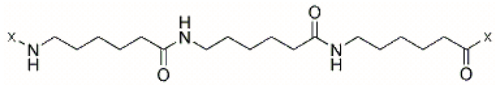

Figure 2.10: Image of a PA6 chain with repeating $C_6H_{11}NO$ parts. [Fig. from [28]]

2.5 Characteristics of Polyamide6/ABS

PA6/ABS consists of polyamide 6 and acrylonitrile-butadiene-styrene and is also a polymer blend like PA6/SAN. Whereas PA6 is a semicrystalline polymer which has a strong chemical resistance and excellent mechanical properties, ABS is a rubber-toughened copolymer with properties that can overcome the drawbacks of PA6 like for example a high sensitivity to notch propagation under impact tests in particular at sub-zero temperatures, high moisture sorption, and a poor dimensional stability [30], [17]. The rubber phase is responsible for improving the toughness of PA6 at low temperatures and SAN provides stiffness, but all in all the thermal stability is lower because of the relatively low glass transition temperature of ABS compared to the melting temperature of PA6 [31]. ABS itself consits of polybutadiene particles dispersed in a styrene acrylonitrile (SAN) matrix and is again included in a matrix of PA6 to form the polymer blend PA6/ABS [32]. One can see its chain structure in figure 2.11. The molecular formula is $(C_8H_8)_n(C_4H_6)_m(C_3H_3N)_l$.

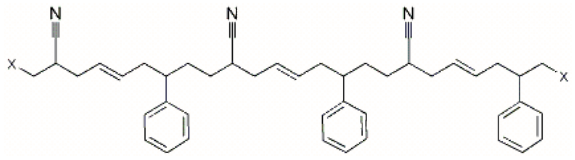

Figure 2.11: Image of an ABS chain with repeating $C_8H_8C_4H_6C_3H_3N$ parts where C_8H_8 is styrene and C_3H_3N is acrylonitrile as in SAN and C_4H_6 is butadiene. [Fig. from [28]]

Whereas PA6 is used for manufacturing for example gear wheels, bearings, and seals, ABS itself is preferred for cases because it builds scratch-resistant surfaces like e.g. Lego bricks [33]. One special use for the PA6/ABS blend is the automotive sector for car interior lining [34].

3 Comparative Studies on PA6/SAN

To demonstrate the new cryo-AFM device's performance and to point out its advantages, images done with the cryo-AFM are compared to images resulting from measurements at the conventional RT-AFM. In addition, sample preparation was done at room temperature and under matched cryo conditions, depending on the requirements of the sample. For measurements the Dimension™ 3100 mentioned in section 2.1.4 was used as RT-AFM. The new cryo-AFM device is "Snotra", built in collaboration with Nano Scan Technology (Moscow, Russia). To complement the discussion, TEM images are added, measured at a Tecnai T12 from FEI (Eindhoven, Netherlands).

3.1 Measurements with a Conventional RT-AFM

Beginning with measurements at the Dimension™ 3100 on PA6/SAN, figures 3.1 and 3.2 show the results. Figure 3.1 includes height ((a) and (b)), amplitude ((c) and (d)) and phase ((e) and (f)) images of the PA6/SAN sample sectioned at room temperature. Since room temperature is not suitable for SAN sample preparation but adequate for the PA6 matrix, the SAN particles got smeared out and are dispersed over the sample towards the cutting direction (recognizable also by knife marks, which are the parallel lines going from the upper left side to the lower right side). Some SAN particles got torn out completely and left huge holes behind. They are visible as completely black parts in the height images. These holes may occur as a problem for scanning with AFM after sample preparation because of big differences in height and steep slopes that lead to an unstable behavior of the cantilever. In addition, one has to

be careful with sample preparation under cryo conditions. After sectioning at room temperature and therefore causing such holes one has to be sure to cut away enough sample material under cryo conditions and ensure that no more parts of the holes appear on the surface.
The described appearance of the sample surface can be seen best in all three images of the 14.58 µm x 14.58 µm scan (figures 3.1 (a), (c) and (e)). Usually the phase image should not contain topography information, but should show a contrast resulting from the different stiffnesses of the two components of the sample. Unfortunately it was not posssible to get one image containing phase contrast after sample preparation of PA6/SAN at room temperature during the whole measurements done for this thesis. The reason therefore is unknown. SAN should definitely be softer than PA6 and changes in the structure through sample preparation can be excluded as an explanation.
Figures 3.1 (b), (d) and (f) show one detail with a scan area 4.17 µm x 4.17 µm of the overview scan. Two holes, one bigger and one smaller, and one small smeared out SAN part embedded in the PA6 matrix are visible. Amplitude images show tiny details like for example the internal ultrastructure of the SAN particles.
Looking at figure 3.2, the images (b), (d) and (f) once again show one detail out of (a), (c) and (e) in height, amplitude and phase. The scan areas are also 14.58 µm x 14.58 µm and 4.17 µm x 4.17 µm. Sample preparation was done at a temperature of -120 °C. AFM measurements took place at room temperature using also the Dimension^{TM} 3100 device. For SAN this temperature of -120 °C leads to nice results since the particles get sectioned smoothly without changing the structure either by deformation through smearing or by compression. So SAN particles appear round and show their internal ultrastructure in AFM measurements. For PA6, on the other side, this sectioning temperature is too low and leads to deformation lines. These lines are also visible in images 2.4 and 2.5 in chapter 2. The reason for this phenomenon has not been solved so far, but [23] offers different models. These models are set up under the assumption that during cutting the sectioned material is periodically collected and shedded away. Deformation lines occuring in ultramicrotomy of plastic material get interpreted by periodic buildup of pressure and friction, alternating with sliding away on the knife surface. Compression occurs, which means a reduction of length in the cutting direction without reduction in the

sample's volume. This increases thickness periodically in lines perpendicular to the cutting direction. Another fact is that a real knife has a finite edge curvature, which results in pressure perpendicular to the upper knife surface. In case of deformation lines, chatter is discriminated from crevasses: chatter is caused by vibrations during cutting while crevasses are the result of bending away of the sections from the sample block [35].
Cutting speed also plays an important role influencing the section quality. But the cutting speed between 0.2 mm s^{-1} and 10 mm s^{-1} does not influence the section morphology, as described in [23]. A distinctly higher cutting speed (e.g. 50 mm s^{-1}) results in chatter lines and tremendous deformations [36]. As we used a speed of 1 mm s^{-1}, deformation lines have their origin in something different, which leads again back to the temperature during cryosectioning which is a definately more sensitive parameter.
In height image (a) of figure 3.2 the topography information is given, showing the deformation lines and the SAN particles which show smaller height information compared to the PA6 matrix. They are somehow contracted and build small recesses. This can be explained by the heating process between sectioning and measuring. When cooled down to -120 °C and sectioned, the sample surface is flat. During heating the sample up again to room temperature the SAN parts start to contract inside the stiffer PA6 matrix due to different coefficients of thermal expansion. The amplitude image (c) once again pronounces small details and the phase image (e) shows the correct phase contrast of harder materials appearing in brighter and softer material in darker color coding.
Three of the SAN particles have lost their bonding to the matrix on one side (the one side where the knife meets them first), visible best in the amplitude image. The internal structure of SAN shows long chains in some parts.
The images on the right hand side of figure 3.2 show fragments of four SAN particles enlarged. This allows to take a closer look at the SAN structure and points out once again all behavior and facts discussed on the images with the larger scanning area.
Looking on the resulting measurements and the surface quality we can easily decide by eye which temperature is adequate for sample preparation of different materials. For example it is obvious that sectioning SAN at room temperature makes no sense whereas at -120 °C we get good results. The sectioning temperature can be adjusted to the glass transition temperature, but

this characterizing parameter strongly depends on the manufacturing process as well as on the cooling rate and can be in addition in a wide range for each polymer. As SAN consists of two different polymers and got mixed with PA6 to a blend, we do not know the glass transition temperatures and have therefore only to decide about the best sectioning temperature by doing experiments.
The deformation lines in PA6, visible e.g. in figure 3.2, of course are the result of the wrong choice of sample preparation temperature for this material. But as we were able to observe, the amount and height of these deformation lines also strongly depend on the sectioned area and the quality of the knife. The smaller the surface area which has to be sectioned and the better the quality of the knife edge, the better the flatness is.

3.2 Measurements with the New Cryo-AFM Device

The new developed cryo-AFM device "Snotra" offers new results in research concerning especially soft materials. To proof the functionality of the system, measurements were done on the same sample used before for conventional AFM scans. As the system allows to operate in a temperature range from -185 °C to 100 °C, first measurements at room temperature were done. The results are expected to be the same as in the equivalent procedure done before at the Dimension^{TM} 3100 when sectioning as well as measuring was done at room temperature.
Figure 3.3 shows the resulting height (a) and phase (b) images of PA6/SAN done at room temperature after sample preparation also at room temperature. This 15.12 µm x 15.12 µm scan is directly comparable to the 14.58 µm x 14.58 µm scan of figure 3.1 and also shows torn and smeared out particles in the height image (a). Since in this particular scan area larger SAN particles are visible, one can nicely observe the internal structure of SAN in particles that did not get deformed by mechanical sample preparation. One can see slight deformations in the polyamide 6 matrix. As mentioned before in section 3.1 the choice of the proper sectioning temperature is not the only guarantor for good surface quality. If the sectioned area is too large and the knife edge contains

marks - and we can actually see some on the images - the PA6 matrix can get deformed because of these factors.
In the phase image 3.3 (b) reverse phase contrast is visible. SAN particles appear brighter in color coding than the PA6 matrix. This phase contrast appearance strongly depends on the angle of the tip to the sample surface. As the tungsten tips, glued on the quartz tuning forks, are hand-made and in addition soldered on the contact plate also by hand, the angle is never exactly 90° but can be much smaller down to 45°. Right now we can assume, looking on our experiments, that the smaller the angle, the higher the probability to get pronounced phase contrast. In the cryo-AFM device the image quality not only depends on the surface quality of the sample and the choice of amplitude parameters A_0 and A_{sp}, but gets influenced also by the length and shape of the tip and its angle to the surface and reacts much more sensitive on the choice of the feedback parameters of the PID-controller.
Figures 3.4 (a) and (b) show the height and phase information after measurements under cryo conditions. In this case PA6/SAN was sectioned and immediately scanned afterwards at a temperature of -80 °C. We did not chose -120 °C, which we used before for sample preparation at RT-AFM measurements, but nevertheless the sample surface appears flat, the choice of -80 °C is also possible for PA6/SAN sample preparation.
Looking at the height image (a) one can see that it suffers from instabilities resulting in horizontal lines across the whole scanned area, but it still shows the internal structure of SAN. Once again, image stability is very sensitive to chosen measuring parameters and the shape of the tip. In addition convection inside the chamber affects the image quality too. During the measuring process the scanning head and the sample can be enclosed in an own capsule but thermal instabilities still have an influence. The most important thing to mention is that now, compared to images (a) and (b) in figure 3.2, SAN parts do not build contracted recesses in the PA6 matrix any more, but appear even higher compared to the matrix. This happens because now we are able to observe the materials exactly in that state in which they have been sectioned and there is no more change in temperature between sample preparation and AFM measurement.
The phase image (figure 3.4 (b)) has a nice phase contrast of softer SAN parts appearing in darker colors compared to the harder PA6 matrix. Some noise

is visible, but with further optimization of parameters the device offers more than satisfying results.

3.3 TEM Images

For TEM measurements a Tecnai T12 was used with an operating voltage of 120 kV and a lanthanum hexaboride (LaB_6) electron source. As investigations with TEM are very well established, comparisons between TEM and AFM images can be helpful and complementary.
Looking at a PA6/SAN sample, one can see SAN particles embedded in the PA6 matrix again quite comparable to AFM images discussed before. Figures 3.5 (a) and (b) show different areas at a section imaged at different magnifications. Deformation lines of high periodicity appear perpendicular to the cutting direction in the PA6 matrix. In this case the sample got sectioned at -120 °C which is too low for PA6 as we also discussed already. No deformation lines are visible in the SAN parts and they are also not round but elliptical in shape because of compression due to too high sectioning temperatures for this material. In addition we are now looking on one thin section which can get deformed in various ways because it gets not stabilized mechanically between the sectioning process and the actual putting on the grid (see section 2.3). This is one advantage of AFM, because in that case the surface always gets stabilized by the rest of the bulk sample. Holes (bright areas) are visible in (a), where SAN got torn out during the sectioning process. Especially in the large SAN particle in the lower left corner of (a) the internal structure is nicely visible. But one should not forget that TEM images are two dimensional projections even when looking on a thin slice of about a few tens of microns.
To get a better contrast in TEM, Osmium Tetroxide (OsO_4), that reacts preferentially with one of the components of the copolymer and gets absorbed, can be used. The presence of the heavy metal Osmium leads to increased Rutherford scattering and therefore to darker areas.
In our case we prepared a wet bath to stain the PA6/SAN sample on TEM grids. To do so, we put some layers of filter paper into a Petri dish and saturated them with distilled water. A glas slide covered with Parafilm was put

onto the filter paper and the grids got positioned on the slide. Close to the grids we put some drops of OsO_4, then closed the dish with another one and waited for two hours. After this staining procedure no changes were observable looking at the samples with TEM (not shown). Staining in the same way as described for another 16 hours showed first results.
In figure 3.6 two different areas of a section of PA6/SAN are shown at again two different magnifications, but both areas were positioned at the margins of the section. This allows us to draw the conclusion that staining starts at the outer edges of the sections to proceed towards the middle. Contrast gets improved with the help of the staining agent especially in case of SAN particles that appeared in the same color grading as the PA6 matrix before staining, although images of unstained areas show the internal structure of SAN quite nicely by comparing figures 3.5 (a) and 3.6 (a) and the contrast of some parts is already good without adding the staining agent.

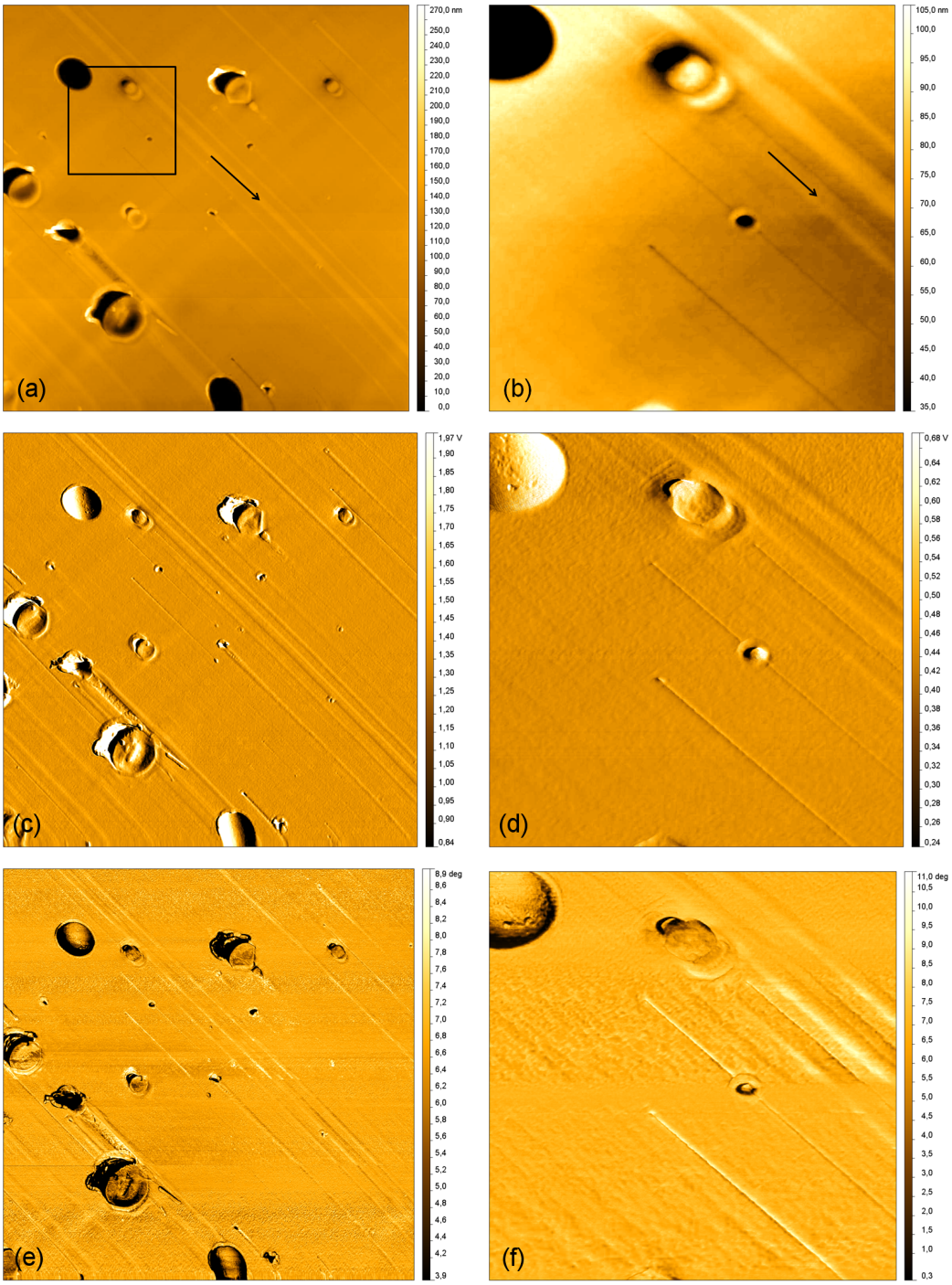

Figure 3.1: Measurement by conventional AFM at room temperature of a PA6/SAN sample sectioned at room temperature; Height (a), amplitude (c) and phase (e) are a 14.58 µm x 14.58 µm scan and (b), (d), (f) are details of (a), (c), (e) in a 4.17 µm x 4.17 µm scan. The scan area for the detailed scan is marked by a black square, the cutting direction is marked by a black arrow.

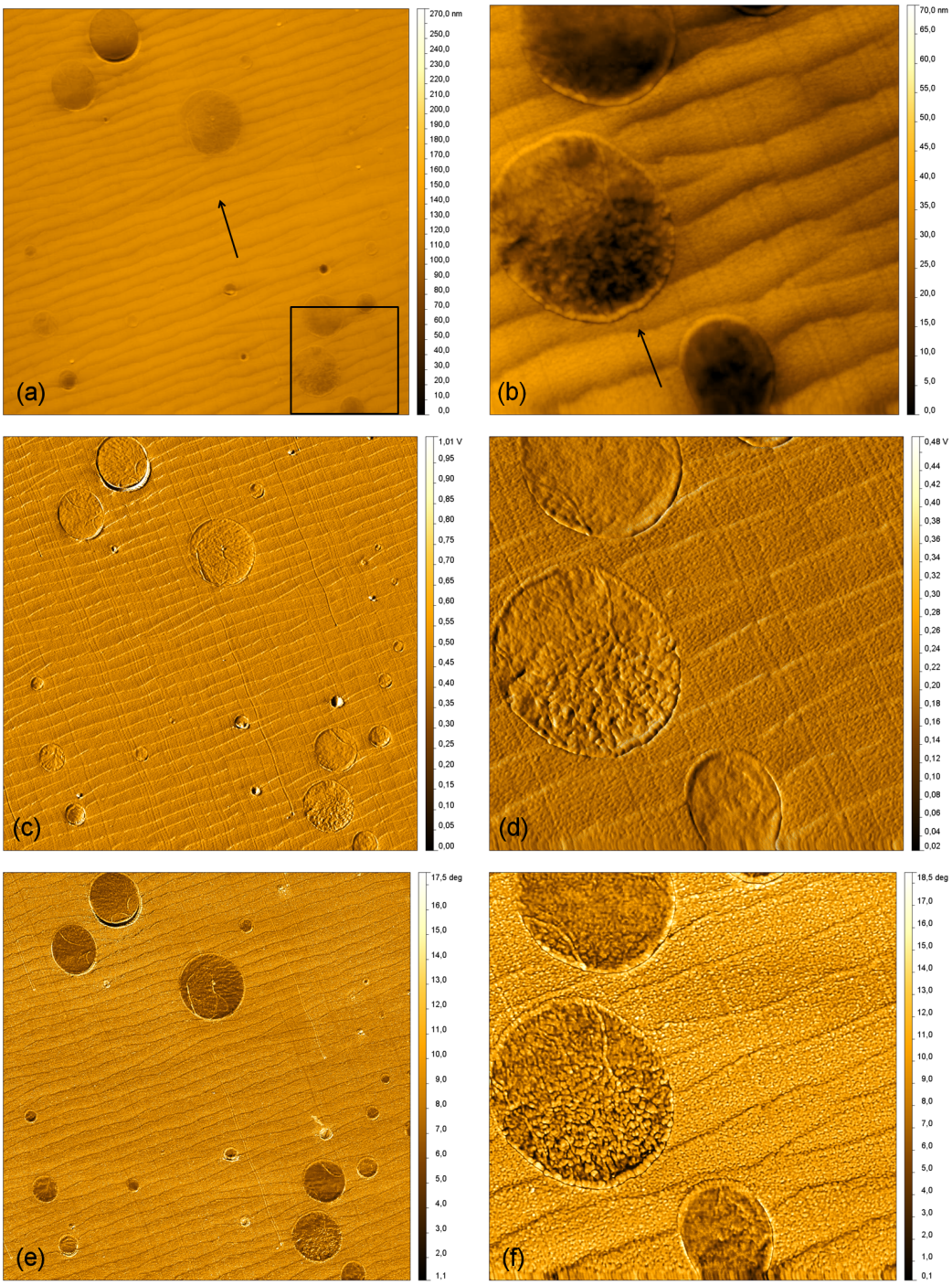

Figure 3.2: Measurement by conventional AFM at room temperature of a PA6/SAN sample sectioned at -120 °C; Height (a), amplitude (c) and phase (e) are a 14.58 µm x 14.58 µm scan and (b), (d), (f) are details of (a), (c), (e) in a 4.17 µm x 4.17 µm scan. The scan area for the detailed scan is marked by a black square, the cutting direction is marked by a black arrow.

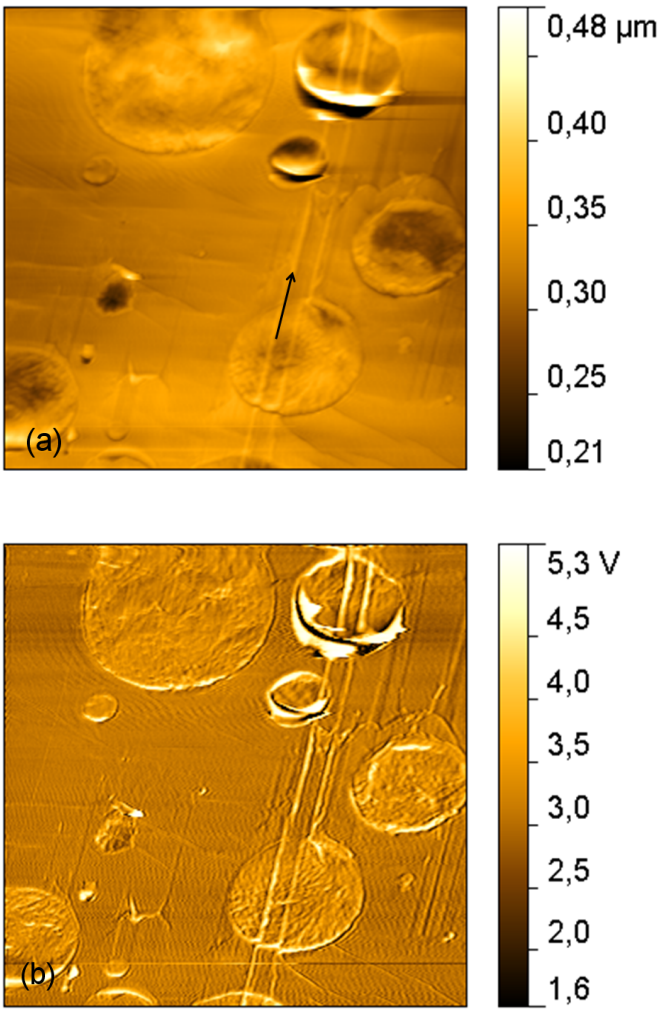

Figure 3.3: Measurement by cryo-AFM at room temperature of a PA6/SAN sample sectioned at room temperature; (a) is the height and (b) the phase information of a 15.12 µm x 15.12 µm scan. The cutting direction is marked by a black arrow.

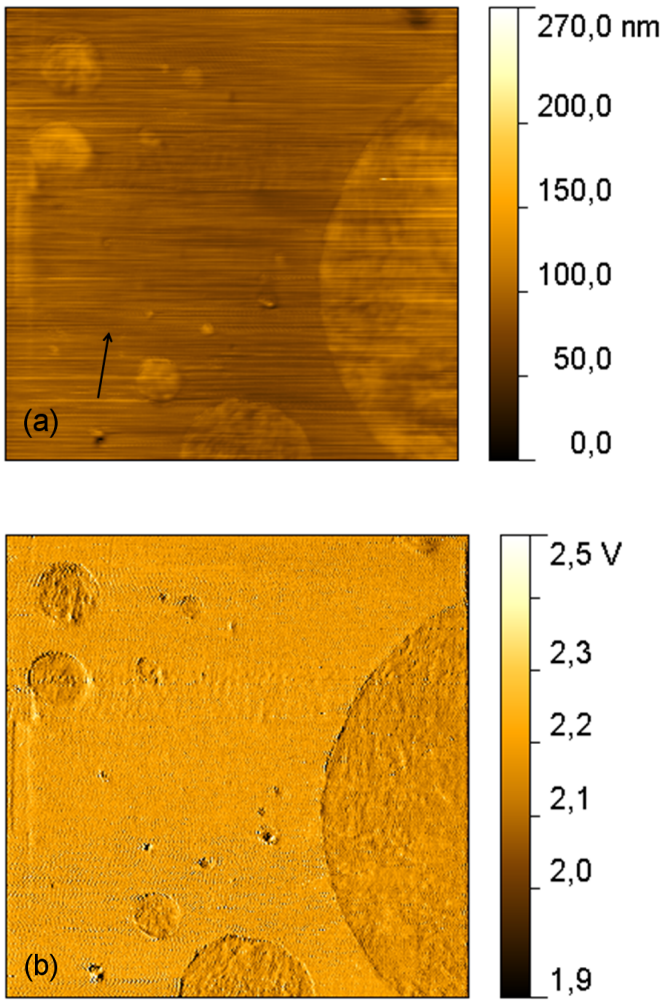

Figure 3.4: Measurement by cryo-AFM at -80 °C of a PA6/SAN sample sectioned at -80 °C; (a) is the height and (b) the phase information of a 11.97 µm x 11.97 µm scan. The cutting direction is marked by a black arrow.

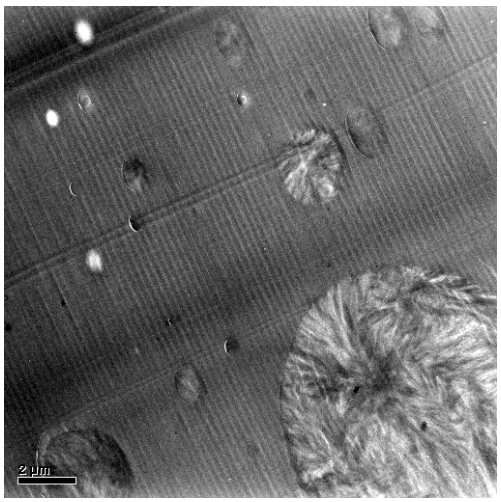

(a) PA6/SAN; Scale bar corresponds to 2 µm

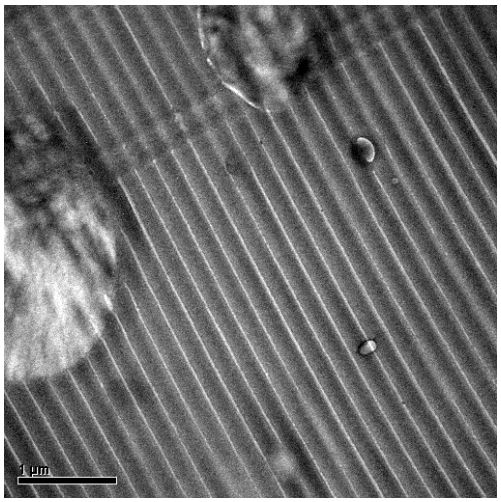

(b) PA6/SAN at higher magnification than in (a); Scale bar corresponds to 1 µm

Figure 3.5: Images of PA6/SAN that got cryo sectioned at -120 °C showing deep deformation lines of high periodicity besides compression of SAN and also knife marks. TEM measurement took place at room temperature.

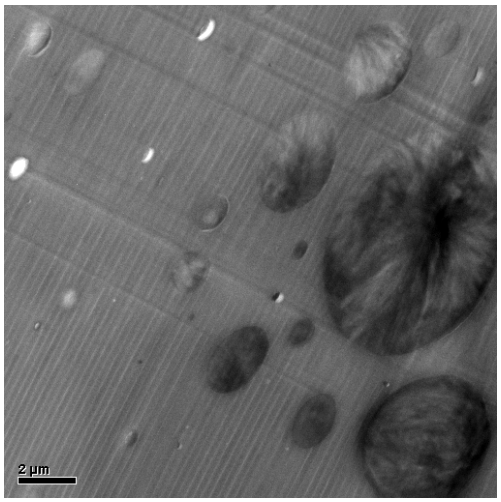

(a) PA6/SAN; Scale bar corresponds to 2 µm

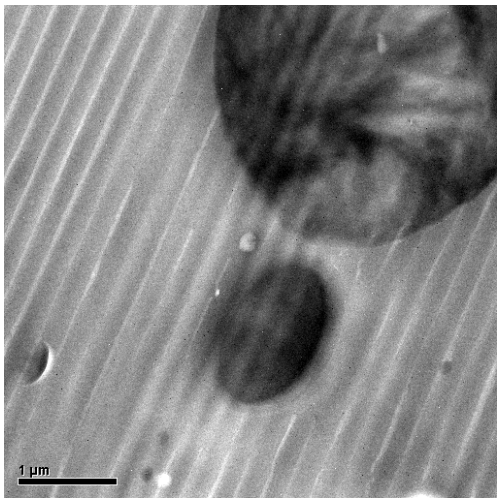

(b) PA6/SAN at higher magnification than in (a); Scale bar corresponds to 1 µm

Figure 3.6: Staining took place at the margins of the section after 18 h in the wet bath with Osmium Tetroxide. Sectioning was done at -120 °C whereas TEM was done at room temperature.

4 Comparative Studies on PA6/ABS

In this chapter images measured at the RT-AFM are shown, afterwards they are compared with results derived from cryo-AFM. Sample preparation was done at room temperature and under cryo conditions to investigate differences. Finally results are complemented by TEM images of sample sections.

4.1 Measurements with a Conventional RT-AFM

Since the multi-phase morphology of PA6/ABS is hard enough to be sectioned at room temperature, figure 4.1 shows images of the sample for its characterization. Images (a), (c) and (e) show height, amplitude and phase and (b), (d) and (f) represent a detailed scan out of the area looked at before. Having a closer look on (a) one will notice that the surface is really flat and almost homogenous. The surface is only covered with low periodic deformations due to the sectioning process perpendicular to the cutting direction. From this image it is visible that especially the borders of ABS particles are slightly higher than the rest of the sample. Amplitude images do not offer much information, but in image (d) the difference in the internal structure of ABS compared to PA6 is obvious, which is something we can see neither in the height nor in the phase image. Phase contrast (seen in (e) and (f)) is optimal, although reversed. ABS is much softer than PA6 and therefore should appear darker than the matrix. In all measurements (except the example shown in figure 2.4 (a)) phase contrast appeared reversed. One can try to force in such cases normal phase contrast by seeking different parameter settings of A_0 and A_{sp}, but since phase was nicely stable, images with reversed phase contrast are presented

here. Nevertheless phase contrast allows to distinguish between the two different components of the two-phase morphology and gives a qualitative analysis of the surface. Quantitatively phase contrast has to be handled with care for the correct interpretation.
The sectioning temperature of about 23 °C is not suitable for the soft ABS, but as it is stabilized by the polyamide 6 matrix, sample preparation at room temperature leads in this case to the good results. As already said in chapter 3, we do not know the glass transition temperature of our samples and their components exactly. The glass transition temperatures of each single polymer influence each other in the block-copolymer. However, slight compressions of ABS particles are observable. The parts are not round but elliptical in shape. Comparing the phase images of figures 4.1 and 4.2 (for 4.2 sample preparation was done at -60 °C) makes the difference apparent.
Sectioning under cryo conditions leads to deformations and crevasses of the PA6 matrix obvious in the height images (a) and (b) of figure 4.2. These deformations do not cause any harm to the morphology and the internal structure of the sample's components (see phase images (e) and (f)). ABS parts are round in shape and dispersed in the same way as seen in figure 4.1. Once again, the actual surface quality and flatness does not only depend on the temperature for sample preparation but gets also influenced by the size of the sectioned area and the quality of the knife edge.
Since the quality of the sample surface of PA6/ABS is much better after sectioning at room temperature, this sample is probably not the best choice for comparison with the new cryo-AFM technique. Nonetheless results of measurements with the cryo-AFM should at least be the same or show what happens with the sample during heating it up to room temperature after cryo-sectioning.

4.2 Measurements with the New Cryo-AFM Device

Cryo sectioning and measuring afterwards under cryo conditions at -60 °C was immediately done after room temperature measurement on the PA6/ABS

sample. This makes sense, because before closing the cryo chamber to prevent ice contamination on the sample surface, the tip or any other part of the system, everything has to be adjusted at room temperature. Doing so, room temperature measurements are self-evident before cooling the device.
The main difference between figures 4.2 and 4.3 is that under cryo conditions ABS parts built contracted recesses that we did not observe in such way at RT-measurements after sectioning at -60 °C. This difference occurs because we look on a sample that did not undergo temperature changes between sample preparation and scanning.
As already observed in figure 3.4 in chapter 3, height images done under cryo conditions suffer from instabilities resulting in lines in the scan direction across the scanned area. To avoid these effects, parameters like the tip and the capsule insulating the actual measuring zone have to be optimized.
Phase information in figure 4.3 (b) gives a correct color coding with darker parts of soft ABS embedded in the harder PA6 matrix and shows even small details of the sample surface. Phase contrast may be more pronounced when the angle between the tip and the surface would be lower, which was already explained in section 3.2.

4.3 TEM Images

Figures 4.4 (a) and (b) show bright ABS parts embedded in a dark PA6 matrix in different magnifications. In this case the sample was sectioned at -80 °C which leads to compression of the softer ABS parts. This results in elliptically shaped ABS instead of parts that are round in shape. Such compression occurs additionally because of the thinness and therefore deformability of the section. Also at -80 °C we see deformation lines perpendicular to the cutting direction (recognizable by the knife mark) in the matrix, that could have appeared during the process of placing the thin section on the TEM grid or might have been avoided on the one hand by elevating the temperature and on the other hand by using a knife of better quality.
Figure 4.4 also gives a nice example of what projection implies: As TEM images are the result of electron signals going through the sample one does not

only investigate the surface of the section but this technique gives a two dimensional projection of the three dimensional section. Therefore ABS parts which lie under a thin layer of the PA6 matrix appear darker and notches appear as bright areas encircled by grey rings. It is obvious that thinner areas or parts with lower atomic number appear brighter in the TEM image because more electrons can get through the objective aperture and lead to a higher signal measured by the CCD camera.
Figure 4.5 (b) shows an area of (a) at higher magnification and in both of them stained and unstained ABS parts are visible. The borderline in-between is distinguishable as a circle. The unstained area has been used before to take TEM images and sustained beam damage. Therefore we can assume that the staining agent is sensitive to beam damage and only an intense staining procedure would stain these parts too which got omitted before. In this case contrast is not so much improved by the staining agent, but the borderlines between ABS and PA6 are highlighted in a better way.

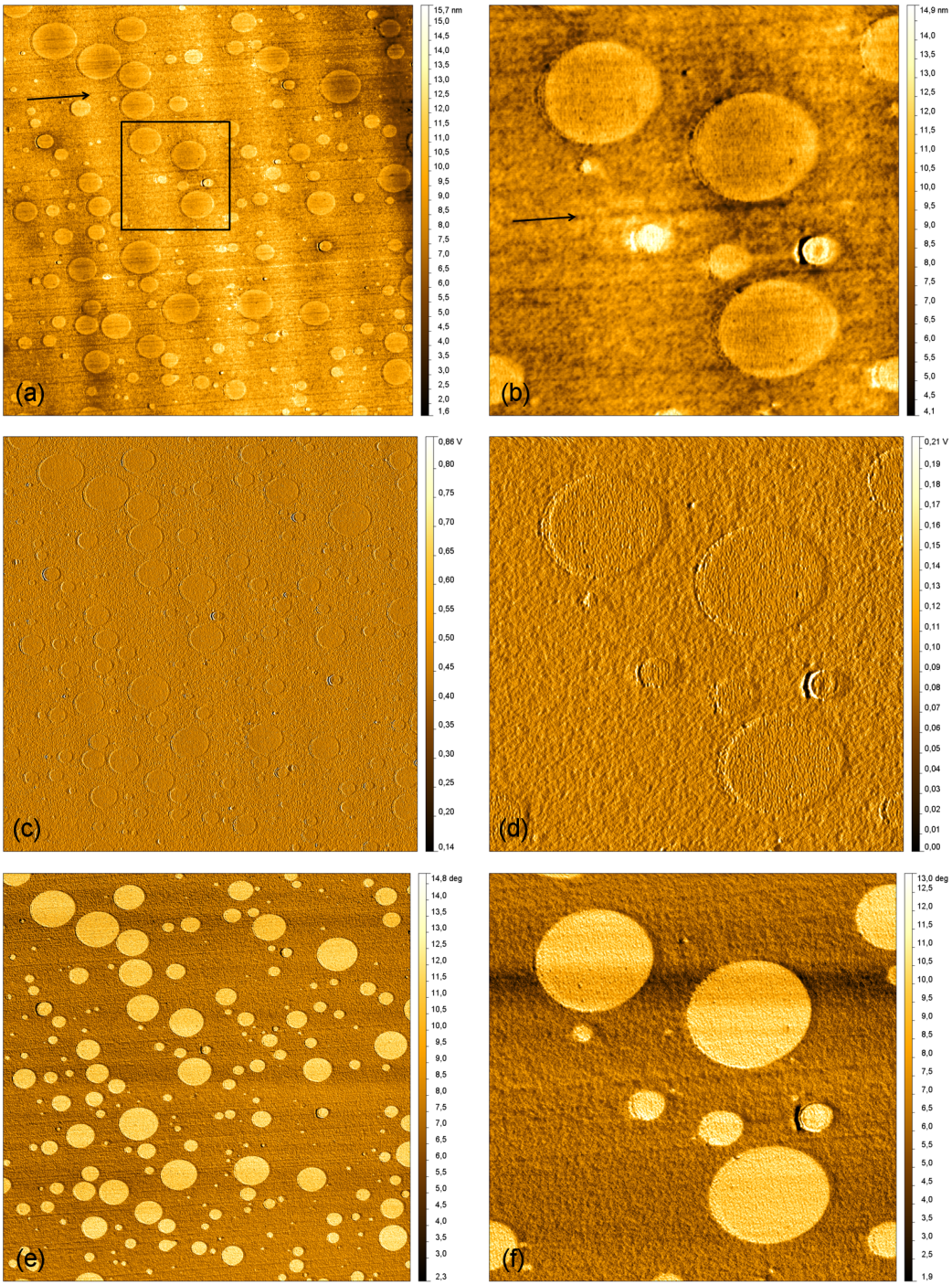

Figure 4.1: Measurement by conventional AFM at room temperature of a PA6/ABS sample sectioned at room temperature; Height (a), amplitude (c) and phase (e) are a 14.58 µm x 14.58 µm scan and (b), (d), (f) are details of (a), (c), (e) in a 4.17 µm x 4.17 µm scan. The scan area for the detailed scan is marked by a black square, the cutting direction is marked by a black arrow.

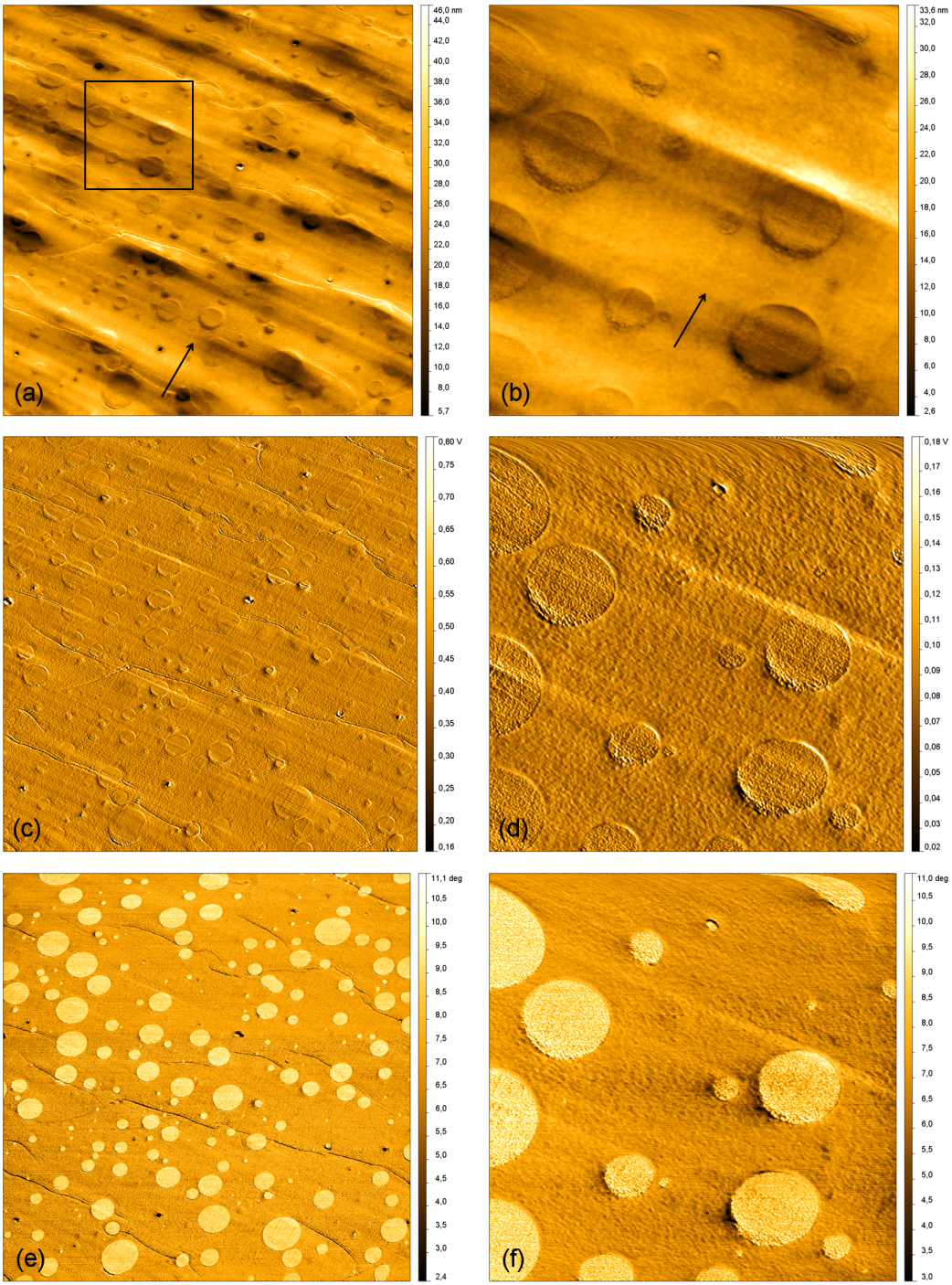

Figure 4.2: Measurement by conventional AFM at room temperature of a PA6/ABS sample sectioned at -60 °C; Height (a), amplitude (c) and phase (e) are a 14.58 µm x 14.58 µm scan and (b), (d), (f) are details of (a), (c), (e) in a 4.17 µm x 4.17 µm scan. The scan area for the detailed scan is marked by a black square, the cutting direction is marked by a black arrow.

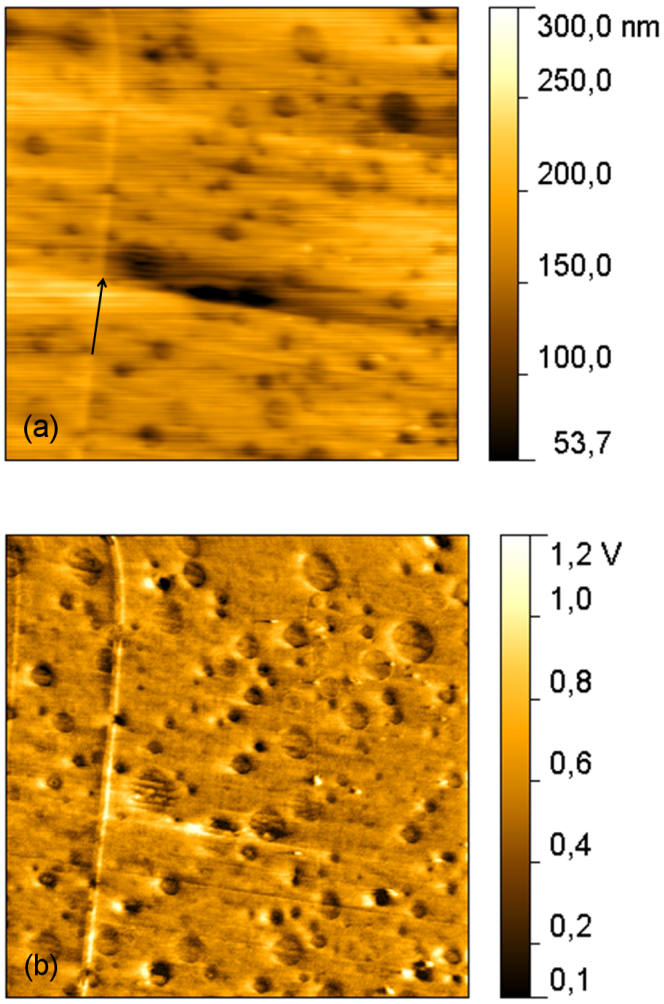

Figure 4.3: Measurement by cryo-AFM at -60 °C of a PA6/ABS sample sectioned at -60 °C; (a) is the height and (b) the phase information of a 12.39 µm x 12.39 µm scan. The cutting direction is marked by a black arrow.

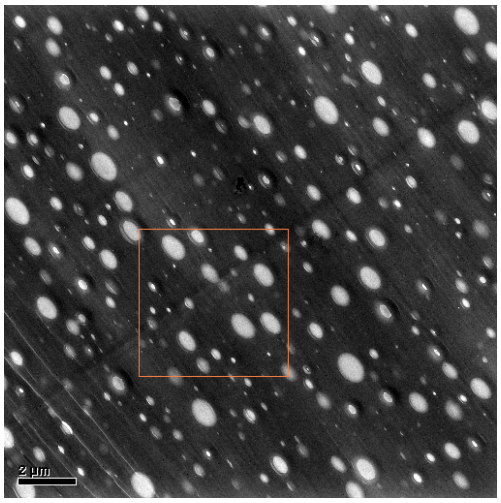

(a) PA6/ABS; Scale bar corresponds to 2 µm

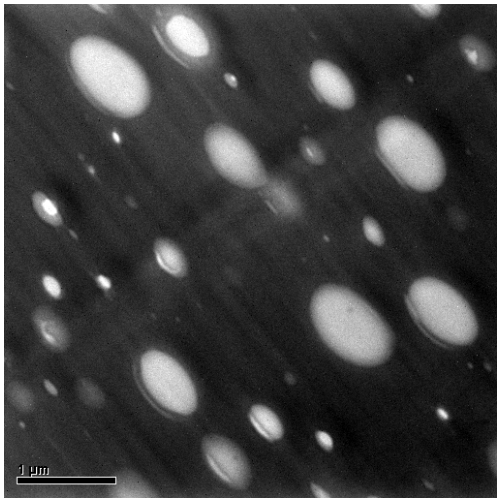

(b) Part of (a) magnified; Scale bar corresponds to 1 µm

Figure 4.4: These images show a PA6/ABS sample which got cryo sectioned at -80 °C and measured at room temperature. One can observe compression, especially at the ABS particles, and knife marks as well as deformation lines.

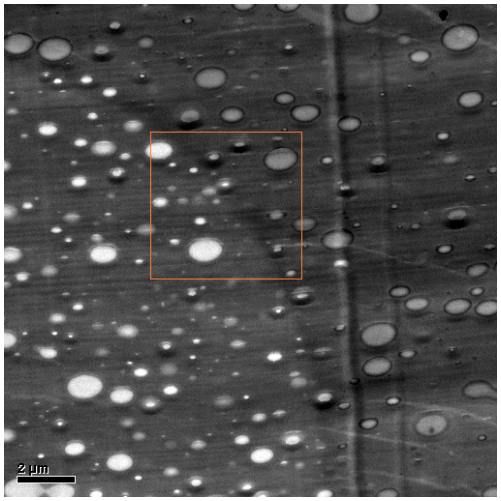

(a) PA6/ABS; Scale bar corresponds to 2 µm

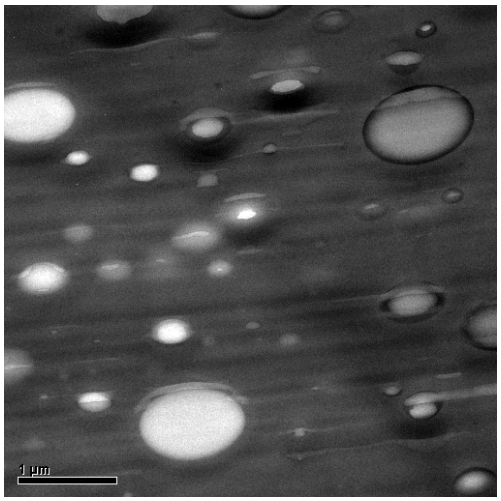

(b) Part of (a) magnified; Scale bar corresponds to 1 µm

Figure 4.5: After altogether 18 h of staining some areas got stained but parts of past beam damage were left unstained. Sectioning was done at -80 °C whereas TEM was done at room temperature.

5 Performance of the Cryo-AFM

To point out the full potential of the new cryo-AFM device different examples are shown. The functionality concerning scanning and resolution is demonstrated on a polyurethane sample and further points out the advantages in comparison to TEM. The second example presents the benefits of measurements under cryo conditions directly after sample preparation at the same temperature and was done on a component of organic and inorganic materials. Finally measurements of two other polymer samples illustrate the possibility of doing three dimensional reconstructions after measurements at room temperature and under cryo conditions. All these specimens have been measured in collaboration with the project team (Dr. Efimov and Dr. Matsko).

5.1 Comparison of AFM Devices

The cryo-AFM is definitely able to keep up with established AFM systems. This shows the comparison of images (a) and (b) in figure 5.1 where (a) images are results from measurements at Dimension^{TM} 3100 and (b) result from scans with “Snotra”. The magnification is different but nevertheless the results are the same. Both times sectioning took place under cryo conditions at -160 °C and measurements were done at room temperature. The images show a polyurethane sample from Voith Paper Rolls GmbH & Co.KG (Wimpassing, Austria). The TEM image (c) shows one part of a sample section where sectioning was done under cryo conditions at -160 °C and TEM took place at room temperature. In this case magnification is even higher compared to AFM images but the contrast of harder spherulite chains dispersed homogenous over the sample surface is low. The reason therefore is on the one hand that both, the spherulites as well as the rest of the sample, are polyurethan only with

some difference in density that leads to contrast. On the other hand the chains do overlap in a network and projection using TEM does not allow to see single chains like we are able to observe when looking at the phase images done by AFM.

5.2 Advantage of Cryo AFM Technology

Another example discusses the advantage of the new possibility to do both, sample preparation and AFM measurement, in the frozen state without any change of temperature in between. We were looking in this case on a sample that consists of silica walls and organic components filled inside those pores. Detailed descriptions can be found in [37]. Figure 5.2 shows one sample made of porous silica walls containing diethylene glycol chains as a carrier material that got filled with monomers. Images (a) and (b) were taken after sectioning at -190 °C by RT-AFM. During observation at room temperature it was not possible to get any information about the organic substance between the silica walls because it contracts inside the carrier material. In contrast, when scanning the sample surface immediately after sample preparation both under cryo conditions, it is the first time we get information about the infiltrated monomers inside their host material visible in the phase image in (c). In this case sample preparation as well as measurements were done at -60 °C.

5.3 3D at Room Temperature

The first step in trying to do serial tomography was to run an experiment at room temperature. A PA6/ABS sample was taken where ABS particles are not necessarily round and in addition have an internal structure with enclosures. Figure 5.3 (a) shows a snapshot of the three dimensional reconstruction created from seven single images. One can see these single measurements in (b). After each measuring step one step of sectioning takes place to go deeper into the

sample. Three dimensional reconstruction was done by Image Pro Plus 6.0 of Media Cybernetics (Bethesda, MD, USA).

5.4 3D under Cryo Conditions

We are also able to do serial sections and measurements under cryo conditions. Because of the fact that measuring under cryo conditions is an advantage when investigating PA6/SAN (see chapter 3), we used this sample. Cryo sectioning and measuring was done at a temperature of -80 °C and a series of six measurements was combined to get the three dimensional reconstruction seen in figure 5.4 (a). In (b) phase (left) and height (right) images are shown.
To do so one has to ensure that everything is adjusted well before closing the cryo chamber of the microtome and cooling down to the desired temperature. After starting the cooling process the chamber should not be opened any more. In case it is necessary, opening is allowed only for short times to prevent the system, especially the tip and the sample surface, from ice contamination and guarantee an equilibrium in temperature and gas flow inside the chamber. Attached ice on the tip changes the resonance frequency as a result of changed mass. Ice on the sample surface does, in this affected parts, not allow to scan properly. Therefore, before starting the cryo procedure, the tip of the probe has to land right in the middle of the sample surface because during sectioning there might appear some drift caused by the first contact of the knife edge with the bulk of the sample and adjustments should allow a high probability to meet the surface again. Further the Q-factor of the tuning fork should not be too high. High Q-factors just allow slow scanning. As a result recording one image within one hour or longer is a disadvantage when measuring such series. During measurements the sectioning is the most challenging part. One has to be careful not to cause drift because we always want to observe the same area of the surface of the specimen even in different layers. Some drift can also be corrected afterwards with the help of software if necessary. Furthermore the section should not attach to the surface again after the sectioning process. Measuring parameters, checked at room temperature, have to be the same for scanning each layer to be comparable and stable. But this does not make sure that the resulting images look the same. Landing is different on each surface

because it is dependend on how the feedback system recognizes it.
The very same has to be considered also for single measurements under cryo conditions but obviously it is less complicated to ensure all alignments only once. However the results (figure 5.4) show that we are able to handle this problems, mainly ice contamination prevention and ensurance of stable temperature and gas flow, and that we do three dimensional reconstructions under cryo conditions.

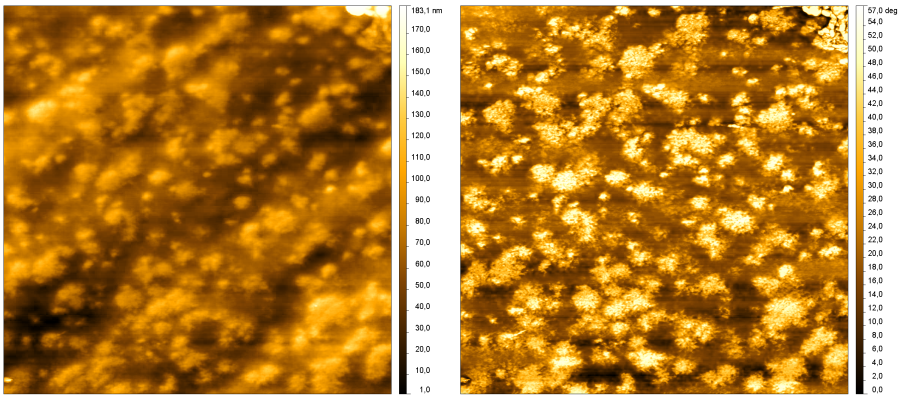

(a) height (left) and phase (right) image measured by RT-AFM after cryo sectioning at -160 °C; 8.6 µm x 8.6 µm scan

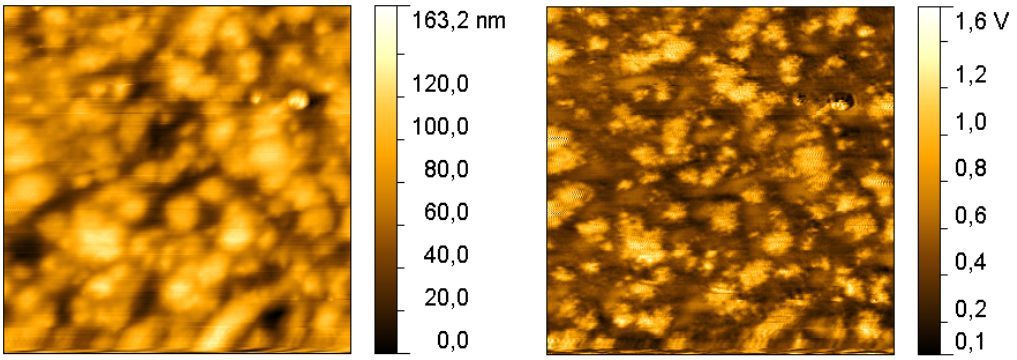

(b) height (left) and phase (right) image measured by cryo-AFM at RT after cryo sectioning at -160 °C; 5.38 µm x 5.38 µm scan

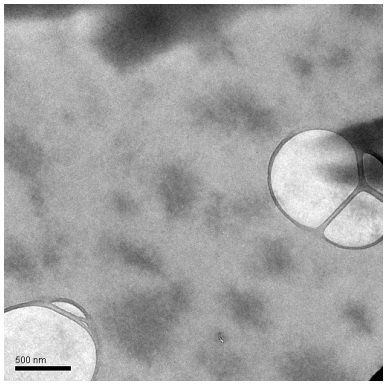

(c) TEM image measured at RT after sectioning at -160 °C; image width=3.43 µm

Figure 5.1: Cryo-AFM measurements offer the same image quality as RT-AFM does. With TEM parts, that are nicely mapped in the phase images of AFM measurements in (a) and (b), show worse contrast due to projection. Sample courtesy of Voith Paper Rolls GmbH & Co.KG (Wimpassing, Austria).

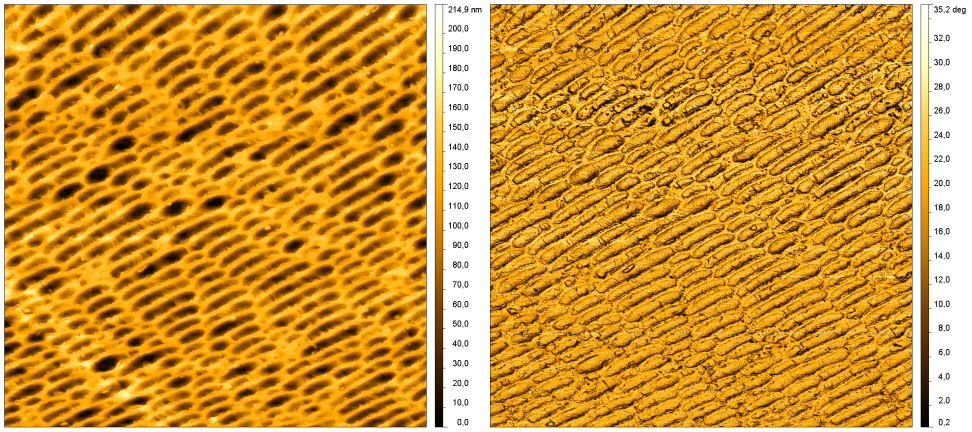

(a) height (left) and phase (right) image measured by RT-AFM after cryo sectioning at -190 °C; 11.35 µm x 11.35 µm scan

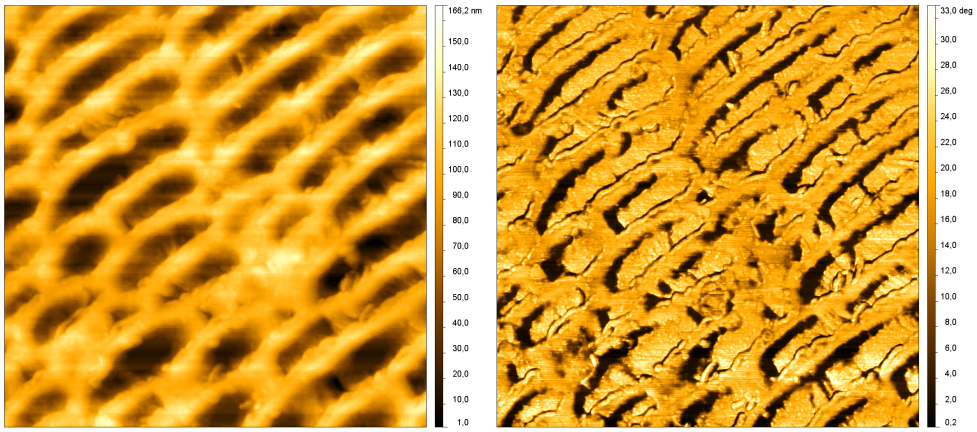

(b) height (left) and phase (right) image measured by RT-AFM after cryo sectioning at -190 °C; 4.17 µm x 4.17 µm scan

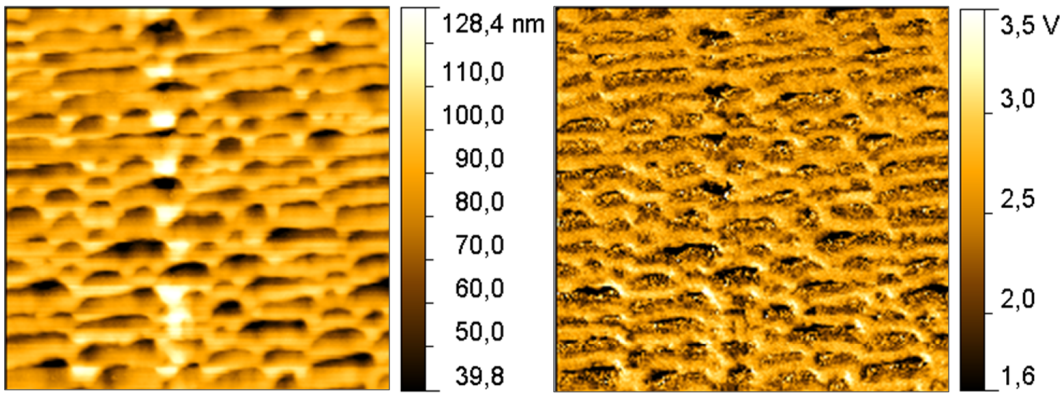

(c) height (left) and phase (right) image measured by cryo-AFM at -60 °C after cryo sectioning also at -60 °C; 3.54 µm x 3.54 µm scan

Figure 5.2: The two images in (b) show a detail of (a). With room temperature measurements it is not possible to get any information about the polymer component between the solid silica walls. With cryo-AFM we get information in the phase image in (c).

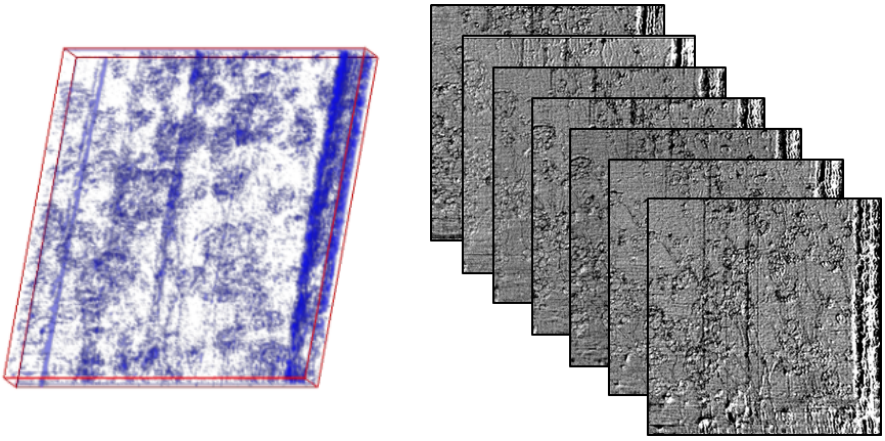

(a) snapshot of the three dimensional reconstruction of a PA6/ABS sample

(b) single frames of phase images used for the reconstruction in (a)

Figure 5.3: The reconstruction consists of seven measurements with an average section thickness of 140 nm. This results in a volume of a size of 12.5 µm x 12.5 µm x 1.0 µm.

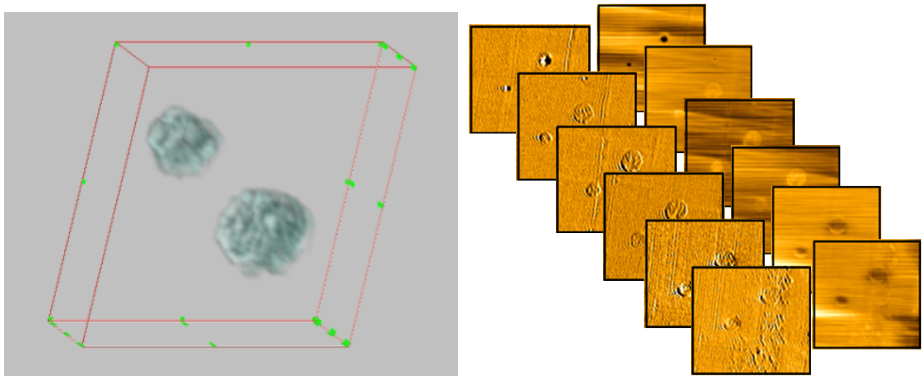

(a) snapshot of the three dimensional reconstruction of the PA6/SAN sample

(b) single frames of phase (left) and height (right) images; phase images were used for the reconstruction in (a)

Figure 5.4: The reconstruction consists of six measurements with an average section thickness of 125 nm. This results in a volume of a size of 3.3 µm x 3.3 µm x 0.75 µm.

6 Conclusions and Outlook

6.1 Conclusions

During the work on this thesis we were sucessful in setting up the new cryo-AFM "Snotra". The system finally gives satisfying results which are discussed in detail in chapters 3, 4 and 5. These chapters also point out the advantages of the new system compared to conventional RT-AFMs like the used Dimension^{TM} 3100. The most obvious benefit is the possibility of in-situ measurements directly after sample preparation at always the same low temperature. This avoids structural changes caused by changes in temperature and it is the first device worldwide that allows to do such experiments.
The final quality of images does depend on various factors:

- The landing and measuring parameters which are the amplitudes A_0 and A_{sp} and the flatness of the sample surface; This is equal to a conventional AFM system.
- The PID-controller settings where the cryo-AFM reacts more sensitively on the choice of parameters than the RT-AFM; Especially the integral term has to be chosen with care.
- The tuning fork; The shape of the tungsten tip, the length, sharpness and the angle to the sample surface strongly influence the stability of the recorded image. Right now the perfect shape gets determined by experiments.

Surface quality, as already mentioned, has a crucial influence on the resulting image because AFM scanners are limited in vertical range of the piezo tube. In addition steep slopes lead to errors of the feedback system and particles or dust on a surface can interrupt the measurement because of loosing contact between the probe and the sample or because of crashing the tip. While

working with soft materials the chosen sample preparation temperature is dependend on the glass transition temperature. However, flat surfaces can only be guaranteed if the sectioned area is small and the knife edge is intact. As we do not know the glass transition temperature of our samples exactly, the proper sample preparation temperature was chosen empirically.
In addition it is possible to do serial section tomography AFM measurements and produce three dimensional reconstructions with "Snotra" at room temperature as well as under cryo conditions. The results are shown in sections 5.3 and 5.4. These new possibilities offer new insights in material characterization that have not been obtained before. AFM-tomography of soft materials will give a new understanding of microstructures and will help researchers to figure out how they are correlated to other sample properties.

6.2 Outlook

The update of the cryo-AFM device is in continuous progress. The goal is to optimize the assembly and the measuring parameters and to make the device more user-friendly.
Further, three dimensional reconstruction measurements on specific examples for nanoliquids, polymers or biological samples will be done under cryo conditions to show the full potential of the device.

7 Appendix

- Verification of calibration:
  The correct calibration of scan area sizes has been verified by measuring a calibration grid with periodicity of 3 µm. Measurements at the Dimension™ 3100 (RT-AFM) and "Snotra" (cryo-AFM), shown in figure 7.1, were done at room temperature. Profiles through one section of the image were done with the programme Gwyddion 2.20 and resulted in the following deviations: The Dimension™ 3100 measures (2.89±0.06) µm instead of 3 µm and "Snotra" measures (2.77±0.05) µm instead of 3 µm.
  As the piezoelement quartz changes with temperature its size and properties, in addition scan sizes have to be recalculated under cryo conditions. Table 7.1 specifies the calibration factors for scale sizes as a function of temperature including factors for room temperature measurements. For scale sizes in images presented in this thesis, factors have already been taken into consideration. Scale size values offered by the software have been divided by the calibration factors to get the correct image size.

Table 7.1: Table of temperature calibration coefficients to rescale measurements done at room temperature and under cryo conditions.
(* Dimension™ 3100, ** "Snotra")

T ...temperature
c.c. ...calibration coefficient

$T/°C$	*c.c.*
*23	0.963
**23	0.923
-60	1.130
-80	1.170
-100	1.215
-120	1.250
-140	1.380

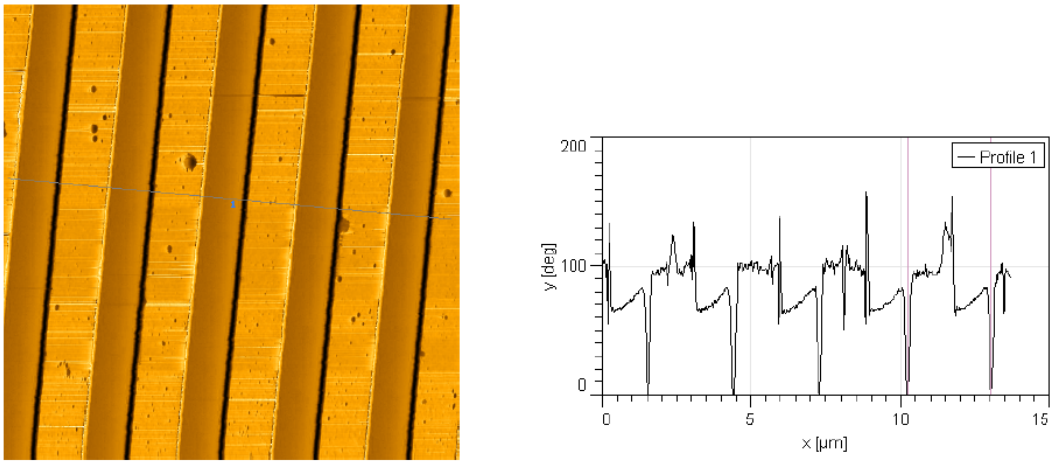

(a) example for grid measurement evaluation at Dimension^{TM} 3100

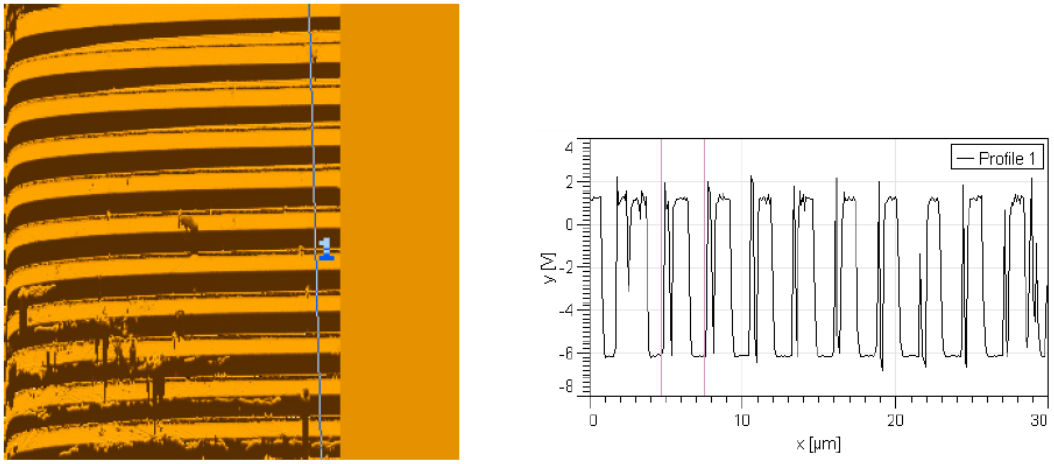

(b) example for grid measurement evaluation at "Snotra"

Figure 7.1: Verification of calibration: on both AFM devices a grid with a known periodicity of 3 µm has been measured.

- Phase images at cryo-AFM:
  Phase images measured with "Snotra" do not have the usual scale in degree units but use volts instead. This is programmed like that in the used software Nspec 7.3 from Nano Scan Technology (Moscow, Russia) and will be changed in the next update. For understanding, the following is valid: the whole range from -180° to 180° (total 360°) corresponds to -10 V to 10 V. This means that 1 V $\equiv$ 18°. Further degree ranges, as a result of RT-AFM and cryo-AFM measurements, are not comparable because the two systems use different mathematical models to calculate

them. Phase images offer a qualitative information which is comparable only in the case of one individual device.

- Section vs. block face:
  The aim of comparing a section used for TEM investigation and the block face surface measured with AFM was to show that the block face surface quality is better than the section itself concerning mechanical stability. This fact is an advantage of AFM studies with easier sample preparation and output of better stability. TEM does not give any information about surface quality but through projection deformation lines are visible as well.
  Sectioning was done by the cryo-ultramicrotome at a temperature of −120 °C, which is too low for the polyamide matrix and therefore leads to periodic deformation lines.
  Comparing a TEM image of a size of 4.84 µm x 4.84 µm (figure 7.2 (a)) with an AFM image of approximately the same size (4.17 µm x 4.17 µm) (figure 7.2 (b)) makes it immediately obvious that there are much more deformation lines on the section than on the block face. In addition the lines on the section show high periodicity and these lines are straight whereas the ones on the block face surface are not periodical and also not straight but they adapt to the SAN particles embedded in the matrix. A closer look on one particular section through each image offers further information. The resulting line profile of the TEM section was calculated by Gatan Digital Micrograph GMS 1.5.1 (Pleasanton, CA, USA), the AFM section got measured by Nanoscope 7.20 of Veeco (Santa Barbara, CA, USA). In each case the distance between two deformation lines was measured by the distance between the contiguous maxima (TEM) or minima (AFM) of each curve. Results are shown in table 7.2. To get better statistics, another section was calculated in an AFM image of 14.58 µm x 14.58 µm in size (figure 7.2 (c)).
  Final results after calculating mean and standard deviation are: distance between the lines on the section observated by TEM: (0.22±0.01) µm and distance between the lines on the block face surface measured by AFM: (0.62±0.05) µm calculated for the 4.17 µm x 4.17 µm scan and (0.7±0.1) µm for the 14.58 µm x 14.58 µm scan. To sum up, the investigated section has deformation lines in closer intervals compared to the

lines appearing on the block face. Because of the thinness of the section the probability of further mechanical deformation after sample preparation is higher than in the case of a block face surface which gets stabilized by the whole bulk of the sample.

Table 7.2: Table of measured distances between deformation lines.

Δmax_{TEM} ...distance between two maxima in the TEM section
Δmin_{AFM_1} ...distance between two minima in the AFM section; fig. 7.2 (b)
Δmin_{AFM_2} ...distance between two minima in the AFM section; fig. 7.2 (c)

Δmax_{TEM} / µm	Δmin_{AFM_1} / µm	Δmin_{AFM_2} / µm
0.2168	0.686	0.874
0.2364	0.638	0.841
0.2168	0.542	0.920
0.2266	0.638	0.713
0.2167		0.761
0.2365		0.634
0.1970		0.713
0.2266		0.793
0.2168		0.841
0.2266		0.333
0.2167		0.793
0.2316		0.682
0.2069		0.745
0.1970		0.841
0.2068		0.888
0.2267		0.888
0.2069		0.539
0.2316		0.508
0.1970		0.666
0.2266		0.555
0.2266		0.745
0.2365		
0.2266		
0.2364		
0.2266		

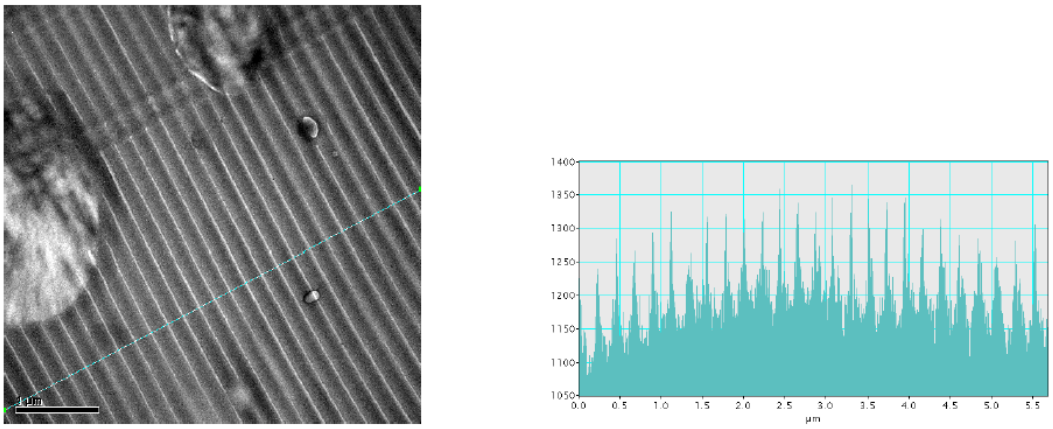

(a) TEM image; scale bar corresponds to 1 µm

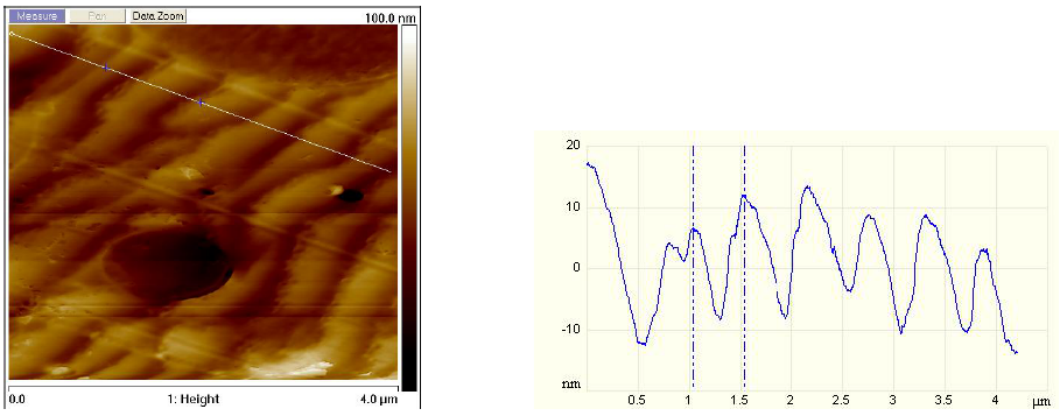

(b) AFM image; 4.17 µm x 4.17 µm scan

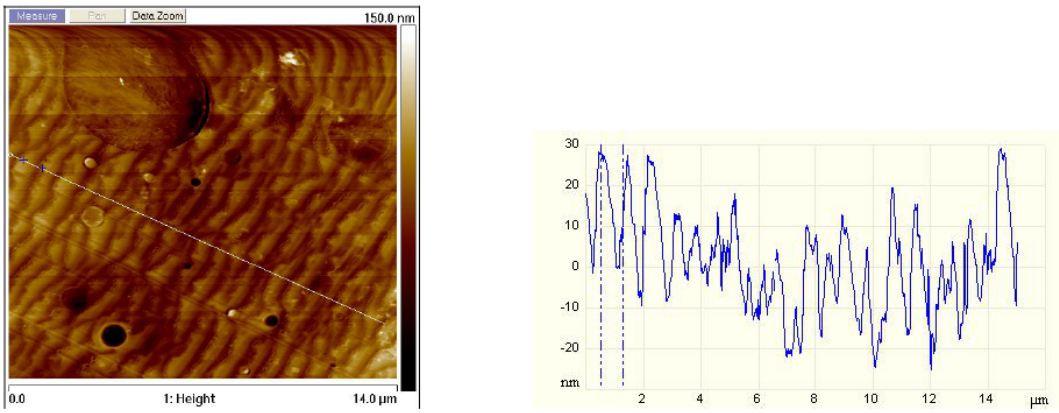

(c) AFM image; 14.58 µm x 14.58 µm scan

Figure 7.2: Comparison of the quality of a section measured with TEM and the block face measured with AFM technique with respect to mechanical stability. The block face surface has less deformation lines in the same area than the section because it gets stabilized by the bulk.

8 Abbreviations

ABS	Acrylonitrile-Butadiene-Styrene
AEM	Analytical Electron Microscopy
AFM	Atomic Force Microscopy
CCD	Charge-Coupled Device
DMSO	Dimethyl Sulfoxide
EDXS	Energy-Dispersive X-ray Spectroscopy
EELS	Electron Energy-Loss Spectroscopy
EFTEM	Energy Filtered Transmission Electron Microscopy
FIB	Focused Ion Beam
PA	Polyamide
PID	Proportional-Integral-Derivative
RT-AFM	Room Temperature Atomic Force Microscopy
SAN	Styrene-Acrylonitrile
SEM	Scanning Electron Microscopy
SPM	Scanning Probe Microscopy
TEM	Transmission Electron Microscopy
UHV	Ultra High Vacuum

Bibliography

[1] V. Mittal, N. B. Matsko, A. Butte, and M. Morbidelli. PNIPAAM Grafted Polymeric Monoliths Synthesized by the Reactive Gelation Process and their Swelling/Deswelling Characteristics. Macromolecular Reaction Engineering, 2:215–221, 2008.

[2] L. C. Sawyer and D.T. Grubb. Polymer Microscopy. Alden Press, Oxford, 2nd edition, 1996.

[3] M. Goh. Advances in Chemical Physics, volume XCI. John Wiley and Sons, New York, 1995.

[4] N. B. Matsko, B. Stadlober, and W. Grogger. Correlative AFM and TEM of Soft Material. About the Synergetic Use of Two Analytical Techniques. Imaging and Microscopy, 10:33–35, 2008.

[5] S. N. Magonov and D. H. Reneker. Characterization of polymer surfaces with atomic force microscopy. Annual Reviews of Material Science, 27:175–222, 1997.

[6] A. E. Efimov, A. G. Tonevitsky, M. Dittrich, and N. B. Matsko. Atomic force microscope (AFM) combined with the ultramicrotome: a novel device for the serial section tomography and AFM/TEM complementary structural analysis of biological and polymer samples. Journal of Microscopy, 226:207–217, 2007.

[7] G. Binnig, C. F. Quate, and C. Gerber. Atomic Force Microscope. Physical Review Letters, 56:930–933, 1986.

[8] S. N. Magonov. Atomic Force Microscopy in Analysis of Polymers. In R. A. Meyers, editor, Encyclopedia of Analytical Chemistry, pages 7432–7491. John Wiley and Sons Ltd, Chichester, 2000.

[9] CarbonNanoprobes. Assembly of an AFM. `http://www.cnprobes.com/tech_afm.htm`, 2009. (Online; accessed February 24, 2010).

[10] F. J. Giessibl. Advances in atomic force microscopy. Reviews of Modern Physics, 75:949–983, 2003.

[11] R. Hoper, T. Gesang, W. Possart, O.-D. Hennemann, and S. Boseck. Imaging elastic sample properties with an atomic force microscope operating in the tapping mode. Ultramicroscopy, 70:17–24, 1995.

[12] U. Duerig, O. Zueger, and A. Stalder. Interaction force detection in scanning probe microscopy: Methods and applications. Journal of Applied Physics, 72:1778–1798, 1992.

[13] K. H. Ang, G. Chong, and Y. Li. PID control system analysis, design, and technology. IEEE Transactions on Control Systems Technology, 13:559–576, 2005.

[14] NT-MDT. SPM principles. `http://www.ntmdt.com/spm-principles/view/semicontact-techniques`, 1998. (Online; accessed December 21, 2009).

[15] J. Israelachvili. Intermolecular & Surface Forces. Academic Press, Singapore, 2nd edition, 1991.

[16] Y. Wang, R. Song, Y. Li, and J. Shen. Understanding tapping-mode atomic force microscopy data on the surface of soft block copolymers. Surface Science, 530:136–148, 2003.

[17] C. F. Sailer. Blends of Polyamide 6 and Styrenic Polymers: Influence of Reactive Compatibilization on Melt Rheology and Morphology. PhD thesis, Eidgenoessische Technische Hochschule Zuerich, 2008.

[18] N. B. Matsko, J. Wagner, A. Efimov, S. Mitsche, W. Czapek, B. Matsko, W. Grogger, and F. Hofer. UFS sensors-32-kHz quartz tuning forks with a long ultra sharp tungsten wire as a tip for the fast scan SPM applications. unpublished, 2009.

[19] N. B. Matsko. private communication.

[20] J.-M. Friedt and E. Carry. Introduction to the quartz tuning fork. American Journal of Physics, 75:415–422, 2007.

[21] J. Rychen, T. Ihn, P. Studerus, A. Herrmann, and K. Ensslin. A low-temperature dynamic mode scanning force microscope operating in high magnetic fields. Review of Scientific Instruments, 70:2765–2768, 1999.

[22] D. A. Ivanov and S. N. Magonov. Atomic Force Microscopy Studies of Semicrystalline Polymers at Variable Temperature. In G. Reiter and J.-U. Sommer, editors, Polymer crystallization, Lecture notes in physics, volume 606, pages 98–130. Springer-Verlag Berlin Heidelberg, 2003.

[23] R. A. Steinbrecht and K. Zierold. Cryotechniques in Biological Electron Microscopy. Springer-Verlag Berlin Heidelberg, 1987.

[24] D. B. Williams and C. B. Carter. Transmission Electron Microscopy, Basics I. Plenum Press New York and London, 1996.

[25] A. Alekseev, A. Efimov, K. Lu, and J. Loos. Three-dimensional Electrical Property Mapping with Nanometer Resolution. Advanced Materials, 21:4915–4919, 2009.

[26] E. A. Nemets, A. E. Efimov, V. A. Egorova, A. G. Tonevitsky, and V. I. Sevastianov. Micro- and Nanostructural Characteristics of 3D Porous Carriers *Elasto*PHB®-3D. Bulletin of Experimental Biology and Medicine, 145:371–373, 2008.

[27] R. A. L. Jones. Soft Condensed Matter. Oxford University Press, New York, 6th edition, 2002.

[28] ChemicalBook. Chemical properties of products. `http://www.chemicalbook.com`, 2008. (Online; accessed February 10, 2010).

[29] L. L. Hou and G. S. Yang. Morphology and Thermal Behavior of MCPA6/SAN Blends Prepared by Anionic Ring-Opening Polymerization of ϵ-caprolactam. Polymer Bulletin, 57:553–561, 2006.

[30] M. I. Kohan. Nylon Plastics Handbook. Carl Hanser Verlag, Munich, 1995.

[31] Y. Li and H. Shimizu. Co-continuous Polyamide 6 (PA6)/Acrylonitrile-Butadiene-Styrene (ABS) Nanocomposites. Macromolecular Rapid Communications, 26:710–715, 2005.

[32] A. Pfau, A. Janke, and W. Heckmann. Determination of the Bulk Structure of Technical Multiphase Polymer Systems with AFM: Comparative AFM and TEM Investigation. Surface and Interface Analysis, 27:410–417, 1999.

[33] LEGO. bricks out of ABS. http://www.lego.com/eng/info/default.asp?page=safety, 2010. (Online; accessed August 02, 2010).

[34] S. Grutke. Zwei ungleiche Brueder vereint. Kunststoffe, 3:108–110, 2006.

[35] K. Richter. Cutting Artefacts on Ultrathin Cryosections of Biological Bulk Specimens. Micron, 25:297–308, 1994.

[36] K. Zierold. The morphology of ultrathin cryosections. Ultramicroscopy, 14:201–209, 1984.

[37] S. Krivec, N. Matsko, V. Satzinger, N. Pucher, N. Galler, T. Koch, V. Schmidt, W. Grogger, R. Liska, and H. C. Lichtenegger. Silica-Based, Organically Modified Host Material for Waveguide Structuring by Two-Photon-Induced Photopolymerization. Advanced Functional Materials, 20:1–9, 2010.